Evaluation of CMIP6 model simulations of $PM_{2.5}$ and its components over China

Fangxuan Ren[1], Jintai Lin[1], Chenghao Xu[1], Jamiu A. Adeniran[1], Jingxu Wang[2], Randall V. Martin[3], Aaron van Donkelaar[3], Melanie S. Hammer[4], Larry W. Horowitz[5], Steven T. Turnock[6, 7], Naga Oshima[8], Jie Zhang[9], Susanne Bauer[10], Kostas Tsigaridis[11, 10], Øyvind Seland[12], Pierre Nabat[13], David Neubauer[14], Gary Strand[15], Twan van Noije[16], Philippe Le Sager[16], Toshihiko Takemura[17]

[1] Laboratory for Climate and Ocean-Atmosphere Studies, Department of Atmospheric and Oceanic Sciences, School of Physics, Peking University, Beijing 100871, China
[2] Frontier Science Center for Deep Ocean Multispheres and Earth System (FDOMES) and Physical Oceanography Laboratory, College of Oceanic and Atmospheric Sciences, Ocean University of China, Qingdao 266100, China
[3] Department of Energy, Environmental, and Chemical Engineering, Washington University, St. Louis, MO, USA
[4] St. Francis Xavier University, Department of Earth Sciences, Antigonish, NS, Canada
[5] NOAA Geophysical Fluid Dynamics Laboratory, Princeton, NJ, USA
[6] Met Office Hadley Center, Exeter, UK
[7] University of Leeds Met Office Strategic (LUMOS) Research Group, University of Leeds, UK
[8] Meteorological Research Institute, Tsukuba, Japan
[9] Beijing Climate Center, China Meteorological Administration, Beijing 100081, China
[10] NASA Goddard Institute for Space Studies, New York, NY, USA
[11] Center for Climate Systems Research, Columbia University, New York, NY, USA
[12] Norwegian Meteorological Institute, P.O. Box 43 Blindern, Oslo, Norway
[13] Centre National de Recherches Météorologiques (CNRM), Météo-France, CNRS, Toulouse, France
[14] Institute of Atmospheric and Climate Science, ETH Zurich, Zurich, Switzerland
[15] Climate and Global Dynamics Laboratory, the National Center for Atmospheric Research, Boulder, CO, USA
[16] Royal Netherlands Meteorological Institute, De Bilt, Netherlands
[17] Research Institute for Applied Mechanics, Kyushu University, Fukuoka, Japan

Correspondence to: Jintai Lin (linjt@pku.edu.cn)

Abstract. Earth system models (ESMs) participating in the latest Coupled Model Intercomparison Project Phase 6 (CMIP6) simulate various components of fine particulate matter ($PM_{2.5}$) as major climate forcers. Yet the model performance for $PM_{2.5}$ components remains little evaluated due in part to lack of observational data. Here, we evaluate near-surface concentrations of $PM_{2.5}$ and its five main components over China as simulated by fourteen CMIP6 models, including organic carbon (OC, available in 14 models), black carbon (BC, 14 models), sulfate (14 models), nitrate (4 models), and ammonium (5 models). For this purpose, we collect observational data between 2000 and 2014 from a satellite-based

dataset for total $PM_{2.5}$ and from 2469 measurement records in the literature for $PM_{2.5}$ components. Seven models output total $PM_{2.5}$ concentrations, and they all underestimate the observed total $PM_{2.5}$ over eastern China, with GFDL-ESM4 (–1.5%) and MPI-ESM-1-2-HAM (–1.1%) exhibiting the smallest biases averaged over the whole country. The other seven models, for which we recalculate total $PM_{2.5}$ from the available components output, underestimate the total $PM_{2.5}$ concentrations, partly because of the missing model representations of nitrate and ammonium. Concentrations of the five individual components are underestimated in almost all models, except that sulfate is overestimated in MPI-ESM-1-2-HAM by 12.6% and in MRI-ESM2-0 by 24.5%. The underestimation is the largest for OC (by –71.2% to –37.8% across the 14 models) and the smallest for BC (–47.9% to –12.1%). The multi-model mean (MMM) reproduces fairly well the observed spatial pattern for OC (R = 0.51), sulfate (R = 0.57), nitrate (R = 0.70) and ammonium (R = 0.~~75~~74), yet the agreement is poorer for BC (R = 0.39). The varying performances of ESMs on total $PM_{2.5}$ and its components have important implications for the modeled magnitude and spatial pattern of aerosol radiative forcing.

1 Introduction

Fine particulate matter ($PM_{2.5}$) influences air quality, human health and climate change. Exposure to near-surface $PM_{2.5}$ is associated with millions of global premature deaths each year (Zhang et al., 2017; World Health Organization, 2021). $PM_{2.5}$ affects the radiative budget of the climate system directly through scattering and absorption and indirectly via clouds. The effects of atmospheric aerosols on cloud droplet concentrations, cloud distributions and radiative properties pose large uncertainties in the estimating radiative forcing (Carslaw et al., 2013; Seinfeld et al., 2016). Earth system models (ESMs) are essential tools for studying global climate change. The accuracy of $PM_{2.5}$ simulations in ESMs exhibits a crucial constraint on the reliability of these models in climate change simulation and projection. The Coupled Model Intercomparison Project Phase 6 (CMIP6) provides an opportunity to evaluate simulated $PM_{2.5}$ and its components by the current-generation ESMs, which implement interactive aerosol and atmospheric chemistry (Turnock et al., 2020). A total of 21 ESMs participating in CMIP6 provide total $PM_{2.5}$ and/or several component simulations, although the aerosol component species vary across these models. Fourteen models include organic aerosol (OA, converted to organic carbon (OC) in this study by assuming OA / OC = 1.6), black carbon (BC), sulfate, dust (DST), and sea salt (SSLT). Four of these

14 models also include nitrate and five include ammonium (Table S1).

Aerosol optical depth (AOD) during 2000–2014 simulated in CMIP5 and CMIP6 are in broad agreement with satellite retrievals over most parts of Europe, North America, and India (Zhang et al., ~~2022~~2022a; Cherian and Quaas, 2020). CMIP6 models better capture satellite-based AOD trends in western North America and eastern China, whereas CMIP5 models failed to reproduce the trends in AOD (Mortier et al., 2020; Cherian and Quaas, 2020). Studies have emerged over recent years to assess the CMIP model performance of individual aerosol components. An assessment of CMIP5 dust aerosol simulations using independent data from 1851 to 2011 over North Africa shows a common underestimate (Evan et al., 2016). Another analysis of CMIP3 and CMIP5 models suggests sea salt aerosols over the tropical Pacific to be significantly underestimated ~~(Chen et al., 2020)~~(Chen et al., 2020). Evaluation of the vertical distribution of BC in CMIP5 models based on aircraft measurements shows an overestimate in the upper troposphere especially over the Central Pacific (Allen and Landuyt, 2014). Several CMIP5 models produce high sulfate burdens over eastern China, the Indian Peninsula and the northern Indo-Chinese Peninsula, although the transport difference among these models results in distinctive spatial distributions (Li et al., 2020). Overall, global climate models struggle to accurately reproduce observed aerosol component concentrations over different world regions.

China is a major region with heavy aerosol pollution, dense population and complex climate, and thus it is critical to understand the performance of ESMs for aerosol simulations over this country. Several studies have evaluated total $PM_{2.5}$ simulations of CMIP models over China, using AOD data from satellite retrievals ~~and ground-based aerosol networks~~ ~~(Mortier et al., 2020;~~ Sockol and Small Griswold, 2017; Michou et al., 2020) and ground-based aerosol networks (Mortier et al., 2020). They find that CMIP5 models reproduce the spatial pattern of AOD reasonably well over eastern China, but with a tendency to underestimate AOD magnitudes (Liu and Liao, 2017; Park et al., 2014; Allen et al., 2013). GFDL-CM3 performs best among CMIP5 models in simulating AOD over eastern China, partly because it includes nitrate and ammonium that most models lack (Li et al., 2020). Other studies suggest that CMIP6 models simulate the magnitude of annual mean AOD better than CMIP5 over eastern China, in part due to the notable increase in sulfate (Cherian and Quaas, 2020; Fan et al., 2018a). ~~Nonetheless, the CMIP6 models fail to capture the seasonal north-south shift of AOD maximum center (Li et al., 2021;~~

~~Wang et al., 2021)~~Nonetheless, the CMIP6 models fail to capture the seasonal north-south shift of AOD maximum center over China during 2000–2014 (Li et al., 2021) and the observed dipole pattern of AOD trends between China and India during 2006–2014 (Wang et al., 2021b).

Formatted: Font color: Text 1

Different $PM_{2.5}$ components exhibit distinctive radiative effects, thus understanding the performance of ESMs in simulating individual $PM_{2.5}$ components is important. Due to the absence of publicly available observational component data over China, only a few studies target single aerosol components (such as sulfate and dust) over a large region of the country, or different $PM_{2.5}$ components over a short period or a small region (Pu and Ginoux, 2018; Zhao et al., 2022). For example, model evaluation based on the Acid Deposition Monitoring Network in East Asia (EANET) suggests that sulfate concentrations simulated by CMIP5 and CMIP6 show a rising trend similar to observations (Mulcahy et al., 2020), but the simulations are still lower than observed concentrations (Fan et al., 2018b; Mortier et al., 2020). A recent study compares $PM_{2.5}$ components (dust, sea salt, BC, OC and sulfate) in CMIP6 models with the Modern Era Retrospective analysis for Research and Applications Aerosol Reanalysis (MERRAero) in Asia from 2005 to 2020 (Su et al., 2022; Buchard et al., 2016). The study shows that CMIP6 model uncertainties of total $PM_{2.5}$ over East Asia are mainly attributable to sulfate and mineral dust simulations. However, the model biases may in part come from other components (nitrate and ammonium) that are not analyzed in their study; and the MERRAero data might contain errors as well (Ma et al., 2021; Mahesh et al., 2019).

In this study, we evaluate near-surface concentrations of $PM_{2.5}$ and its five main components (OC, BC, sulfate, nitrate, and ammonium) from 2000 to 2014 over China simulated by fourteen CMIP6 models driven by historical emissions. For this purpose, we employ a satellite-based dataset for total $PM_{2.5}$ concentrations and a self-compiled $PM_{2.5}$ component dataset from 221 ground stations during 2000–2014 collected from the literature. Section 2 introduces CMIP6 model simulations, satellite-based total $PM_{2.5}$ concentration data, and literature-based $PM_{2.5}$ component data. Section 3 assesses the performance of CMIP6 models for total $PM_{2.5}$. Section 4 evaluates the simulated $PM_{2.5}$ components. Section 5 discusses the climate implications of the inadequacies in total $PM_{2.5}$ and its components in CMIP6 models. Section 6 concludes the study.

2 Data and method

2.1 CMIP6 simulations

Near-surface concentrations of total $PM_{2.5}$ and its components can be converted from dry aerosol mass mixing ratios (MMRs) in CMIP6 models. Monthly mean near-surface MMRs (in the lowest model layer) of $PM_{2.5}$ and its main components are taken from fourteen CMIP6 models to assess the performance of ESMs over China (Table S1). Data are obtained from the "Historical" experiments covering 1850−2014, which serve as the entry cards for participating in CMIP6 (Eyring et al., 2016). They are coupled atmosphere-ocean simulations that include all CMIP6 historical forcings, and are well suited for quantifying and understanding model characteristics. The ensemble mean is taken for each model by averaging all available ensemble members. For GISS models, the ensemble members use two physics configurations with drastically different aerosol parameterizations. We average the ensemble members using the same physics configurations in GISS models, named GISS-E2-1-OMA (physics-version = 3) and GISS-E2-1-MATRIX (physics-version = 5) respectively (Bauer et al., 2020). Simulation results over 2000−2014 are selected and re-gridded to 1° × 1° for comparison with available satellite- and ground-based data.

The anthropogenic emission data (ver. 2016-07-26) to drive "Historical" CMIP6 simulations is produced by the Community Emissions Data System (CEDS) (Hoesly et al., 2018). An updated version of CEDS (ver. 2017-05-18) corrected several errors in the spatial distribution within each country, but does not change total emissions by country and sector (Feng et al., 2020). The CEDS emissions (ver. 2016-07-26 and ver. 2017-05-18) of OC, BC, CO, NO_x and SO_2 in China after 2000 are higher than those in the Multi-resolution Emission Inventory for China (i.e., MEIC) (Paulot et al., 2018; Zheng et al., 2018) ~~inventory~~ and the Peking University (PKU) inventory (Wang et al., 2014; Huang et al., 2015; Tao et al., 2018) which use more detailed Chinese data. This difference in China has been reduced when CEDS was used to derive future SSP scenarios in CMIP6 simulations (published on ESGF on 28 June 2018 on https://esgf-node.llnl.gov/search/cmip6), and has been included in a post-CMIP6 version of CEDS ~~(McDuffie et al., 2020)~~(McDuffie et al., 2020).

Of the fourteen models, all output the MMRs of OA, BC, sulfate, dust and sea salt, five output ammonium, and four output nitrate (Table S1). Seven models output the MMRs of total $PM_{2.5}$, as the sum over all

components with suitable particle sizes. The MMRs are converted to mass concentrations (μg m^{-3}) based on air density in each model. In evaluating $PM_{2.5}$ components (Sect. ~~2.3), modeled~~4), the evaluation of dust and sea salt concentrations is excluded due to the lack of available ground-based observations. We compare OC, BC, sulfate, nitrate, and ammonium simulations with the observed data available for these components. Modeled OA is converted to organic carbon (OC) to be comparable with the observational dataset. Modeled OA refers to total organic aerosol, including primary organic aerosol (POA) and secondary organic aerosol (SOA). For the GFDL-ESM4 model, the "mmroa" variable for OA only includes POA; thus we calculate the total OA of GFDL-ESM4 as mmroa plus mmrsoa. The OA/OC ratios in the literature range from 1.4 to 2.1 (Bürki et al., 2020; Lin et al., 2016). We choose an OA/OC ratio of 1.6, which is the same as the ratio used in converting near-surface OA observations to OC. This ratio is slightly higher than the value of 1.4 recommended by CMIP6 for POA, but it does not affect the relative (percentage) model bias found in this study because the same ratio is used for models and observations.

For the seven models that do not output total $PM_{2.5}$, we follow the previous work to estimate total $PM_{2.5}$ concentrations (Eq. 1) (Turnock et al., 2020). Here, OA, BC, sulfate and certain portions of sea salt (SSLT, a_1) and dust (DST, a_2) are assumed to be present in fine particles (diameter < 2.5 μm).

$$PM_{2.5} = OA + BC + SO_4^{2-} + a_1 \times SSLT + a_2 \times DST \quad (1)$$

For most models, specific values of a_1 and a_2 are provided by model developers (Table S2). BCC-ESM1 does not provide the coefficients. Instead, the model outputs concentrations in four size bins for each of dust (DST01: 0.1−1.0 μm, DST02: 1.0−2.5 μm, DST03: 2.5−5.0 μm, and DST04: 5.0−10 μm) and sea salt (SSLT01: 0.2−1.0 μm, SSLT02: 1.0−3.0 μm, SSLT03: 3.0−10 μm, and SSLT04: 10−20 μm) (Su et al., 2022; Wu et al., 2019). Thus, the first two bins are assumed to belong to $PM_{2.5}$. Ammonium and nitrate are not available in most of these six models (except GISS-E2-1-MATRIX) and are thus not included in Eq.1.

2.2 Satellite-based total $PM_{2.5}$

We take satellite-based near-surface total $PM_{2.5}$ concentrations from the V4.CH.03 product of the Washington University Atmospheric Composition Analysis Group ~~(Hammer et al., 2020)~~(Hammer et al.,

Formatted: Space After: 12 pt

2020). The dataset is constructed by combining multiple satellite products of AOD with simulations from a chemical transport model (GEOS-Chem) to predict $PM_{2.5}$, and then constraining these estimates by ground-level $PM_{2.5}$ monitoring. ~~It provides the annual average $PM_{2.5}$ concentrations during 2000–2014 with a high spatial resolution of 0.01° × 0.01° (~1 × 1 km^2).~~The GEOS-Chem aerosol simulations include primary and secondary carbonaceous aerosols, sulfate, nitrate, ammonium, mineral dust, and sea salt. The dataset provides the annual average $PM_{2.5}$ concentrations during the period 2000–2014 with a high spatial resolution of 0.01° × 0.01° (~1 × 1 km^2). The adjusted satellite-derived $PM_{2.5}$ concentrations over Asia are compared with surface $PM_{2.5}$ observations collected from the Global Burden of Disease (GBD) collaborators during the period 2008–2013 ($Mean_{satellite}$ = 61.5 μg m^{-3} versus $Mean_{obs}$ = 59.1 μg m^{-3}) (van Donkelaar et al., 2016) and from the China National Environmental Monitoring Center (CNEMC) during the period 2015–2019 ($Mean_{satellite}$ = 45.9 μg m^{-3} versus $Mean_{obs}$ = 43.4 μg m^{-3}) (van Donkelaar et al., 2021). Detailed data descriptions are provided elsewhere (van Donkelaar et al., 2019; van Donkelaar et al., 2016). Here the satellite-based total $PM_{2.5}$ data are re-gridded to 1° × 1° for model evaluation purposes.

Formatted: Font color: Auto

2.3 Ground-based $PM_{2.5}$ components data

Since national-scale continuous measurements of near-surface $PM_{2.5}$ components are unavailable in China, we collect observational $PM_{2.5}$ component data from the literature. Our collected dataset includes 2469 component records of OC, BC, sulfate, nitrate, and ammonium nationwide (627, 66, 645, and 1131 records in western regions, Northeast China, North China, and Central and South China, respectively), as shown in Figure 1. Here a record represents one measured $PM_{2.5}$ component at the specific sample site and period. These records cover 30 provinces (including provinces and provincial-level municipalities) and multiple land use types (urban, rural, near the road, and industrial park, etc.). The dataset does not cover Ningxia, Guizhou, Heilongjiang, and Taiwan. A total of 472, 459, 518, 519, and 501 records are available for OC, BC, sulfate, nitrate, and ammonium over China, respectively. The site locations, sampling periods, data sources, and other information are summarized in the Supplement.

At a given site, the records are not continuous in time. These records cover varying sampling periods ranging from a few days to several years, although most are monthly data. We treat a record as seasonal if its data length is equal to or shorter than a season, or as annual when its data length is longer than 6 months. The records are not evenly scattered across years and are more available in later years in general.

From 2000 to 2008, the numbers of records range from 50 to 150 per year, except for 2003 (207 records); while from 2009 to 2014, the numbers of records vary between 150 to 550 per year (Fig. S1). To compare with CMIP6 simulations, we calculate for each site the multi-year mean $PM_{2.5}$ component concentrations by averaging over the seasonal or annual observational records. If there are more than one sites in a given model grid cell, we average data from all sites in that grid cell. To consider the effect of interannual variability~~,~~ (caused by incomplete temporal match in data availability between models and observations), we compute for each CMIP6 model the average and maximum of annual mean values ~~over~~during 2000–2014 from all grid cells with available observational data, and then compare with the multi-year averaged observations from these grid cells. As detailed in Section 5, the model biases are not caused by imperfect model-observation matching in time.

3 Evaluation of near-surface total $PM_{2.5}$

3.1 Spatial distribution

The spatial distribution of satellite-based annual mean total $PM_{2.5}$ concentrations (Fig. 2 p) exhibits high values over populous and industrial North China (including Beijing, Tianjin, Hebei, Shandong, and Shanxi provinces, 52.6 μg m^{-3}) and eastern Sichuan (60.9 μg m^{-3}). Central and South China exhibits $PM_{2.5}$ concentrations (46.5 μg m^{-3}) lower than North China, due to lower emissions, higher vegetation coverage, better ventilation conditions and more precipitation. $PM_{2.5}$ concentrations are modest over dusty southern Xinjiang (33.6 μg m^{-3}). Low $PM_{2.5}$ concentrations (< 8 μg m^{-3}) are distributed over the plateaus or forested regions with small populations, such as Tibet and northern Heilongjiang. Overall, $PM_{2.5}$ concentrations in the south and coastal regions are lower than in the northern and inland regions.

Among the seven models that directly output total $PM_{2.5}$ concentrations (Fig. 2 a-g), GFDL-ESM4 and MPI-ESM-1-2-HAM show similar patterns and magnitudes to satellite data with small national average biases (–1.5% and –1.1%, respectively~~).~~) because of better performance in BC, sulfate, and ammonium simulations (Fig. S4-S7), which are related to the aerosol-chemistry-climate schemes within CMIP6 models (Turnock et al., 2020). Over the eastern regions (including Northeast China, North China, and Central and South China), all models exhibit spatially averaged negative biases ranging from by –47.9% to –3.3~~%.~~% (Fig. S2). Nevertheless, the spatial pattern over the eastern regions is well simulated by four models (GFDL-ESM4, GISS-E2-1-OMA, MIROC-ES2L, and MPI-ESM-1-2-HAM) (R > 0.9, as shown

in Table S2) with the maximum center over North China correctly reproduced. Over the western regions, four models (GFDL-ESM4, MRI-ESM2-0, NorESM2-LM, and NorESM2-MM) reproduce the maximum center over southern Xinjiang, although each of the seven models can underestimate or overestimate the peak values substantially.

For the seven models with total $PM_{2.5}$ derived from Eq.1, their simulated $PM_{2.5}$ concentrations underestimate the satellite-based data by –65.5% to –48.0% averaged over the country (Fig.2 h-n). The negative biases are in part because nitrate and ammonium are not included ~~(10.4–17.2~~. About 15.1–20.6% and ~~10.1–~~11.~~14~~–14.6% of $PM_{2.5}$ are nitrate and ammonium in the models that do contain them~~).~~, as shown in Table S3. Over the eastern regions, HadGEM3-GC31-LL and UKESM1-0-LL exhibit the least underestimation, and they also capture the observed maximum center over North China. Five of these seven models do not reproduce the $PM_{2.5}$ peaks over dusty regions in the west, pointing to model deficiencies in dust simulations (Zhao et al., 2022).

Formatted

3.2 Trend and interannual variability

Over the eastern regions (Northeast China, North China, and Central and South China), data from satellite (0.72 μg m^{-3} yr^{-1}) and all models (0.32–1.14 μg m^{-3} yr^{-1}) exhibit significant increases (p-value < 0.05) in annual mean total $PM_{2.5}$ concentrations over 2000–2014, with temporal correlation between 0.63 and 0.87 (Fig. 3 a and Table S2). The positive trend of satellite data over the eastern regions is consistent with findings from previous studies (de Leeuw et al., 2022; Geng et al., 2021) , as caused mainly by emission changes (Hoesly et al., 2018; Wang et al., 2022). GFDL-ESM4 and MPI-ESM1-2-HAM exhibit annual average $PM_{2.5}$ concentrations and trends similar to the satellite data since 2004. Regionally, the fourteen models capture the interannual variations of satellite $PM_{2.5}$ over Northeast China ($R > 0.9$) and North China ($R > 0.8$) (Fig. 4). The temporal consistency reflects that the models capture the temporal changes in anthropogenic emissions over these polluted regions, although the models might not align with natural (meteorology-driven) variability.

Over the western regions where natural dust dominates the aerosol loadings, satellite-based $PM_{2.5}$ concentrations experience no significant trend over 2000–2014, whereas 11 models increase significantly ranging from 0.10–0.28 μg m^{-3} yr^{-1}) (Fig. 3 b). ~~The notable decline over 2000–2005 in satellite data (–~~

~~1.12 μg m^{-3} yr^{-1}), which reaches 90% confidence level but no 95%, is not captured by any model.~~There is a notable decline over 2000–2005 in satellite data (–1.12 μg m^{-3} yr^{-1}, at the significance level of 0.1) consistent with the previous studies that use dust aerosol optical depth (DOD) and ground-based observations of dust storm (Wang et al., 2021a; Song et al., 2016). However, the dramatic drop is not captured by any model, reflecting large uncertainties and inter-model diversities in dust simulations stemming from many factors such as the driving mechanisms, dust particle size, and model structural differences (Zhao et al., 2022). Over 2000–2014, NorESM2-LM, NorESM2-MM, and MPI-ESM-1-2-HAM show large interannual variations whereas other models do not. The models do not align with the yearly changes found in the satellite data, with modestly positive, low or even negative correlation coefficients (–0.6 to 0.6, Fig. 4). The inaccuracy in aerosol trend and variability might exert erroneous forcing upon the climate system.

4 Evaluation of near-surface $PM_{2.5}$ components

4.1 Organic carbon and black carbon

Ground-based observations of carbonaceous aerosols (OC and BC) are mostly available in the eastern regions. The national average multi-year mean observed OC concentration reaches 15.9 μg m^{-3}. Observed OC concentrations peak over North China (> 25 μg m^{-3}) and are also high over Central and South China (5–25 μg m^{-3}) (Fig. 5 a). The national average of the 14-model mean (6.5 μg m^{-3}, normalized mean bias (NMB) = –59.0%), which ~~are~~is spatially coincidently sampled with the ground-based observations~~,~~ (i.e., model values are obtained from grid cells with available observations), severely underestimates the observations, especially over parts of North China with the bias reaching –40 μg m^{-3} (Fig. 5 b). Nevertheless, the spatial pattern of OC observations is captured by the 14-model mean modestly well with a correlation coefficient of 0.51. Further, a negative bias exceeding –50% occurs in 11 models, even though they can simulate the spatial pattern moderately well (R ranges from 0.40 to 0.58, Fig. ~~S2). The discrepancy of OC between models peaks over North China and eastern Sichuan, as shown in Figure 5 c.~~S4).

The national average multi-year mean observed BC concentration is 4.3 μg m^{-3}. Observed BC concentrations are high (> 10 μg m^{-3}) over parts of North China with mining and other heavy industries, such as Hebei and Shanxi province (Fig. 5 d). However, the 14-model mean (3 μg m^{-3}) does not capture

Formatted: Space After: 12 pt

the spatial pattern very well (R = 0.39) and it underestimates the observations (NMB = –27.2%). The 14-model mean presents the largest negative bias over Shanxi (–15.2 μg m^{-3}) and the greatest positive bias over Shandong (3.9 μg m^{-3}, Fig. 5 e); both provinces are in North China. Twelve of the 14 models underestimate the BC observations (by –47.9% to –12.1% for national average), whereas two models (HadGEM3-GC31-LL and UKESM1-0-LL) exhibit positive biases (by 21.1% and 26.2%, respectively) (Fig. 6 and Fig. ~~S3~~S5). Most models produce high concentrations of BC over the whole North China, including Beijing and Shandong that exhibit relatively low observational values. The spatial distributions of carbonaceous aerosol concentrations are mainly influenced by CEDS emissions used in models, with higher spatial correlation coefficients greater than 0.85 (Fig. S3).

The underestimation of carbonaceous aerosol concentrations might be associated with anthropogenic emissions, chemical mechanisms, and meteorological conditions. ~~The~~ For China, the CEDS emission data (ver. 2016-07-26) used in CMIP6 historical simulations are ~~overestimated~~about 3.8–31.3% higher than those in ~~China.~~MEIC inventory except for NO_x emissions (Fan et al., 2022). However, the positive bias in emissions cannot explain the model underestimation of OC and BC concentrations. ~~Instead, the~~The model inadequacies in chemical processes (e.g.~~,~~, using simplified aerosols and chemistry schemes, which tends to underestimate ~~–~~aerosol formation~~)~~ (Turnock et al., 2020)~~,~~) might lead to underestimated secondary organic aerosols (SOA~~) concentrations,~~, as a component of OC), especially over Central and South China ~~(Chen et al., 2016).~~(Chen et al., 2016). The inter-model discrepancies of OC and BC peak over North China and eastern Sichuan (Fig. 5 c). The large absolute discrepancies are in part due to the higher air pollutant concentrations in these regions. Furthermore, many differences exist among CMIP6 models in $PM_{2.5}$ component simulations, including the representation of aerosol size distribution; the simplification of chemical processes with photolytic, kinetic and heterogeneous reactions (e.g., 33 photolytic reactions in BCC-ESM1 but 43 in GFDL-ESM4) (Turnock et al., 2020; Wu et al., 2020b; Dunne et al., 2020); the treatment for transport of gaseous tracers and aerosols by advection and vertical convection; and the dry deposition and wet scavenging schemes (Su et al., 2022; Digby et al., 2024).

Meteorological conditions, including temperature, precipitation and surface wind simulations, have critical impacts on local aerosol concentrations. Temperature simulations over the eastern regions of China by CMIP6 models are very close to the observed data ~~(Yang et al., 2021).~~(Yang et al., 2021). Over

Formatted: Space Before: 0 pt

Formatted: Font color: Text 1

the western regions, a notable warm bias over Xinjiang in most CMIP6 models (Zhang et al., 2022b) may contribute to higher planetary boundary layer height (Yue et al., 2021) and stronger vertical mixing, partly explaining the underestimation of OC and BC concentrations near the surface (Fig. 5); whereas the pronounced cold bias over the Tibetan Plateau (Zhu and Yang, 2020) might contribute to overestimated near-surface aerosol concentrations over there. Precipitation affects aerosol concentrations through wet scavenging; and it is overestimated (wet bias) in CMIP6 models over North China and Northeast China but close to observations over Central and South China ~~(Yang et al., 2021)~~(Yang et al., 2021). The model performance in precipitation may partly explain the more severe underestimation of OC concentrations over North China than over Central and South China. But the overestimation of BC over North China suggests that other factors offset the influence of local wet bias. Over the western regions, most models exhibit wet bias, except over northern Xinjiang where local temperature (warm bias) and precipitation (dry bias) have opposite effects on near-surface aerosol concentrations. Furthermore, the overall underestimation of surface wind speed over China in CMIP6 (Wu et al., ~~2020~~2020a) is conducive to the accumulation of near-surface aerosol concentrations around the anthropogenic emission source regions, which may induce a negative contribution to the underestimation of OC and BC concentrations.

Field Code Changed

4.2 Sulfate, nitrate and ammonium

This section evaluates the model performance of secondary inorganic aerosols (sulfate, nitrate, and ammonium; SIOA). Sulfate aerosol in CMIP6 models is dependent on SO_2 emissions (the main sulfuric acid precursor), chemical conversion of SO_2 to sulfate, and loss through wet scavenging (Wu et al., 2020b; Tegen et al., 2019). Some models also explicitly simulate nitrate and ammonium aerosols using the sulfate-nitrate-ammonia thermodynamic equilibrium. For instance, EC-Earth3-AerChem, GISS-E2-1-MATRAX and GISS-E2-1-OMA use the Equilibrium Simplified Aerosol Model (EQSAM) (Metzger et al., 2002; Bauer et al., 2020; van Noije et al., 2021), while GFDL-ESM4 treats ammonium and nitrate aerosols with ISORROPIA (Fountoukis and Nenes, 2007; Paulot et al., 2016; Dunne et al., 2020).

Formatted: Pattern: Clear

Formatted: Pattern: Clear

The national average multi-year mean of observed sulfate concentrations reaches 14.6 μg m^{-3}, the second largest value among the five $PM_{2.5}$ components (following OC). The observed sulfate concentrations exceed 15 μg m^{-3} over most of North China and eastern Sichuan, as well as cities over Xinjiang with

large population and petroleum industry (Fig. 5 g). The 14-model mean, whose national average is 9.3 μg m^{-3}, has the greatest underestimation over North China and Xinjiang (Fig. 5 h). The 14-model mean agrees modestly well with the observations in spatial pattern (R = 0.57). Among the 14 models, the national average model biases range from –66.1% (GISS-E2-1-OMA) to 24.5% (MRI-ESM2-0); and five models better capture the observed spatial pattern with correlation coefficients exceeding 0.6 (Fig. 6). The cross-model discrepancy in sulfate (2 μg m^{-3} in national average) is larger than those for the other four components (0.4–0.9 μg m^{-3}), particularly over Central and South China (Fig. 5 i).

The national average multi-year mean of observational nitrate concentrations is 8.7 μg m^{-3}. The observed spatial pattern of nitrate is similar to sulfate, with high values over North China, eastern Sichuan and populous cities of Xinjiang (Fig. 5 j). Only four models (GFDL-ESM4, GISS-E2-1-OMA, GISS-E2-1-MATRIX, and EC-Earth3-AerChem) include nitrate simulations. The 4-model mean has a national average of 5.5 μg m^{-3}, with a NMB of –36.5%; but it captures the observed spatial pattern very well with a correlation coefficient reaching 0.7. All the four models exhibit negative NMBs ranging from –41.4% to –25.4%; they reproduce high values over the eastern regions but have underestimation over Xinjiang (Fig. ~~S5~~S7).

The observed multi-year mean ammonium concentrations have a national average value of 6.7 μg m^{-3}. The observational values peak over North China (> 10 μg m^{-3}), particularly over the agricultural regions from which ammonia emissions are the greatest (Fig. 5 m). Five models perform ammonium simulations. The 5-model mean, with a national average of 3.4 μg m^{-3}, has negative and positive biases between –12.2 and 1.5 μg m^{-3} at different locations (Fig. 5 n). The 5-model mean captures the observed spatial pattern of ammonium (R = 0.74) better than for other components (R = 0.39–0.70). The five models exhibit varying performances in magnitude and spatial pattern. The NMBs range from –89.0% to –13.6% across these models. Four models simulate the spatial patterns of ammonium well with high correlation coefficients between 0.67 to 0.76, although the spatial agreement is poor for CESM2-WACCM (R = 0.21).

Emissions, meteorological conditions and chemical processes affect the formation and loss of secondary inorganic aerosols. As explained in Sect. 4.1, the potentially overestimated CEDS emissions over China, the cold bias over the Tibetan Plateau, and the dry bias over northern Xinjiang tend to overestimate

aerosol concentrations, which are in contrast with the negative model biases over the respective regions. On the other hand, the warm bias over northern Xinjiang and the wet bias over North China and Northeast China are in line with the underestimation of aerosol concentrations. Furthermore, the formation of nitrate from nitric acid depends on the amount of residual ammonia left from the formation of ammonium sulfate. Over the regions where ammonia is not sufficient to neutralize both nitric acid and sulfuric acid (such as Shanxi and Shandong), decreased sulfate formation might promote nitrate formation with the released ammonium (Zhai et al., 2019; Zhai et al., 2021). This partly explains why the underestimation of nitrate simulations is less than sulfate over these regions.

5 Discussion

Over the eastern regions, the concentrations of total $PM_{2.5}$ and its five components are underestimated by the 14 models in general. The slight underestimation of three models (GFDL-ESM4, MPI-ESM-1-2-HAM, and MRI-ESM2-0) can be traced to positive biases in sulfate simulations partly offsetting the negative biases in OC and BC. Over the western regions, most models underestimate the total $PM_{2.5}$ concentrations dominated by dust aerosols, whereas three models (GFDL-ESM4, NorESM2-LM, and NorESM2-MM) produce overly high values over Xinjiang due to overestimated dust concentrations. Meanwhile, all models underestimate the five $PM_{2.5}$ components over the west.

Figure 7 shows little difference between the maximum and average annual concentrations over 2000–2014 for national mean $PM_{2.5}$ components simulated by individual models. Furthermore, we average over all seasonal and annual observational records to compare with annual mean model results. A test using the seasonal (annual) model results to match seasonal (annual) observational records shows very similar comparison results (Fig. ~~S6~~S8). These tests suggest that the model underestimation cannot be attributed to imperfect temporal matching between models and observations or the potential mis-phase (or variability) in models.

Among the five $PM_{2.5}$ components evaluated, absorbing aerosol (BC) and four scattering aerosols (OC, sulfate, nitrate, and ammonium) have opposite direct radiative forcing at the top of atmosphere (TOA). The underestimation of BC is less than for the other four scattering aerosols. If this difference persists in the troposphere, the underestimated $PM_{2.5}$ components might cause an underestimation of negative

radiative forcing at TOA. The underestimation of BC and scatter aerosols might result in more solar radiation reaching the ground (Chen et al., 2022; Tang et al., 2022). This is consistent with the overestimation of maximum daily maximum temperature over the eastern regions ~~(Zhu et al., 2020)~~(Zhu et al., 2020), likely serving as a positive feedback between negative aerosol biases and overestimated surface temperature.

The spatial biases in aerosols might also serve as an important limiting factor for the performance of meteorological/climate simulations. The observed $PM_{2.5}$ and its five components are characterized by high concentrations over the east and low values over the west (except northern Xinjiang). In a few models, the large overestimation of $PM_{2.5}$ over Xinjiang of the west (dominated by dust) with underestimated $PM_{2.5}$ (dominated by anthropogenic aerosols) over the east might exert an incorrect west-east asymmetric climate forcing. The spatial pattern of resulting climate response might include cold-warm biases of surface temperature (cold bias over the west and warm bias over the east). The difference in the spatial pattern of model bias between BC and scattering aerosols might have additional impacts on the climate. Future work is needed to examine how the model errors in $PM_{2.5}$ and its components might affect climate simulations through aerosol-climate feedback.

6 Summary

In this study, we evaluate the performance of 14 CMIP6 ESMs in simulating total near-surface $PM_{2.5}$ and its five components over China during 2000–2014, and discuss the likely causes for model errors, and their climate implications. Our assessment helps to understand the capability of the current-generation models in the simulation of aerosols and aerosol-climate interactions, towards further improvement of climate predictions and projections. Our findings are summarized as follows:

(1) Twelve of the 14 CMIP6 models tend to underestimate the total $PM_{2.5}$ concentrations over China (NMB = –65.5% to –1.1%) and the other two models overestimate them (NMB = 17.0%–39.2%), as compared to a satellite-based dataset. The seven models that output total $PM_{2.5}$ concentrations exhibit underestimation between –47.9% and –3.3% over the eastern regions, although four of them capture the observed spatial pattern ($R > 0.9$). Over the western regions, four of these seven models reproduce the maximum center over southern Xinjiang. The seven models, for which we calculate the total $PM_{2.5}$

concentrations from outputted components, underestimate the observed $PM_{2.5}$ by –65.5% to –48.0% averaged over the country, in part due to missing nitrate and ammonium in the models.

(2) Over the eastern regions, all models simulate significant increasing trends of total $PM_{2.5}$ (0.32–1.14 μg m^{-3} yr^{-1}) over 2000–2014 that are close to satellite-based data (0.72 μg m^{-3} yr^{-1}). The models also capture the interannual variability of satellite $PM_{2.5}$ over Northeast China and North China. Over the western regions, 11 models simulate growing $PM_{2.5}$ concentrations at rates of 0.10–0.28 μg m^{-3} yr^{-1}, in contrast to no significant trends in satellite data.

(3) The 14-model mean captures the spatial pattern of observed OC modestly well (R = 0.51), but it exhibits severe underestimation nationwide (NMB = –59.0%), with negative biases exceeding –50% in 11 models. The 14-model mean shows a poor capability in capturing the BC spatial pattern (R = 0.39), and it also underestimates the BC observations (NMB = –27.2%). Two models exhibit positive biases in BC, while the other 12 models exhibit negative biases.

(4) Fourteen, four and five models output the sulfate, nitrate, and ammonium, respectively. The 14-model mean of sulfate exhibits modest spatial correlation and bias (R = 0.57, NMB = –36.5%); and there exist large discrepancies among these models, with biases ranging from –66.1% to 24.5%. The 4-model mean of nitrate captures the spatial pattern well (R = 0.7), although it still underestimates concentrations nationwide (NMB = –36.5%). The 5-model mean of ammonium has the best performance in reproducing the spatial pattern (R = 0.74) but with a negative bias in magnitudes (NMB = –46.5%).

(5) The overall underestimation of $PM_{2.5}$ and its components are associated with imperfectness in emissions as input, modeled meteorology and chemistry. The underestimated $PM_{2.5}$ and its components might cause an overall underestimated cooling effect at TOA and stronger warming at the surface in the models. The model performance in spatial pattern differs between BC and scattering aerosols; and a few models also exhibit strong positive biases over the west (associated with dust) but negative biases over the east. Together, the errors in spatial pattern might have additional consequences for the modeled climate. Further studies are warranted to quantify how model errors in the magnitude and spatial pattern of aerosols affect the regional and global climate, for example, through the Regional Aerosol Model Intercomparison Project (RAMIP) (Wilcox et al., 2022).

As a final note, those causes for aerosol underestimation may also affect ozone, and the underestimated aerosol concentrations might also further affect the ozone simulation through radiative or heterogeneous chemical processes (Jacob, 2000; Lin et al., 2012; Li et al., 2019). In addition, as CMIP6 models are also used to study the health impacts of aerosols (Xu et al., 2022; Shim et al., 2021), the aerosol underestimation needs to be corrected to allow a more reliable estimate of health consequences.

Data availability

CMIP6 data are available on the Earth System Grid Federation (ESGF) and can be freely downloaded via the website interface https://esgf-data.dkrz.de/search/cmip6-dkrz/ (last access: 8 September 2020, WCRP, 2020). Satellite-derived surface $PM_{2.5}$ concentration products can be accessed from the Washington University Atmospheric Composition Analysis Group website as version V4.CH.03 at https://sites.wustl.edu/acag/datasets/surface-pm2-5/. Observational data used in this paper are provided in the SI, with raw data available upon request to the corresponding author Jintai Lin (linjt@pku.edu.cn).

Author contributions

JL led the study. FR and JL designed the study, analyzed the results, and wrote the paper. CX provided the map data of four regions in China. JA collected observation data of $PM_{2.5}$ components from the literature. JW helped to analyze the evaluation results. RM, AD and MH provided satellite-derived data of total $PM_{2.5}$. ST performed UKESM1-0-LL and HadGEM3-GC31-LL simulations. NO performed MRI-ESM2-0 simulations. JZ performed BCC-ESM1 simulations. SB and KT performed GISS-E2-1-OMA and GISS-E2-1-MATRIX simulations. ØS performed NorESM2-LM and NorESM2-MM simulations. PN performed CNRM-ESM2-1 simulations. DN performed MPI-ESM1-2-HAM simulations. GS performed CESM2-WACCM simulations. TN and PS performed EC-Earth3-AerChem simulations. LH performed GFDL-ESM4 simulations. TT performed MIROC-ES2L simulations. All authors commented on the manuscript.

Competing interests

The authors declare that they have no conflict of interests.

Financial support

Jintai Lin and Fangxuan Ren have been supported by the National Natural Science Foundation of China (grant no. 42075175) and the second Tibetan Plateau Scientific Expedition and Research Program 525 (grant no. 2019QZKK0604). Naga Oshima has been supported by the Environment Research and Technology Development Fund (grant nos. JPMEERF20202003 and JPMEERF20232001) of the Environmental Restoration and Conservation Agency provided by Ministry of the Environment of Japan, the Arctic Challenge for Sustainability II (ArCS II, grant no. JPMXD1420318865), and the Global Environmental Research Coordination System from Ministry of the Environment, Japan (grant no. MLIT2253). David Neubauer has been supported by the European Union's Horizon 2020 research and innovation programme project (FORCeS, grant no. 821205). Randall Martin has been supported by NASA (grant no. 80NSSC21K0508).

Reference

Allen, R. J. and Landuyt, W.: The vertical distribution of black carbon in CMIP5 models: Comparison to observations and the importance of convective transport, J. Geophys. Res. Atmos., 119, 4808-4835, https://doi.org/10.1002/2014JD021595, 2014.

Allen, R. J., Norris, J. R., and Wild, M.: Evaluation of multidecadal variability in CMIP5 surface solar radiation and inferred underestimation of aerosol direct effects over Europe, China, Japan, and India, J. Geophys. Res. Atmos., 118, 6311-6336, https://doi.org/10.1002/jgrd.50426, 2013.

Bauer, S. E., Tsigaridis, K., Faluvegi, G., Kelley, M., Lo, K. K., Miller, R. L., Nazarenko, L., Schmidt, G. A., and Wu, J.: Historical (1850–2014) Aerosol Evolution and Role on Climate Forcing Using the GISS ModelE2.1 Contribution to CMIP6, J. Adv. Model. Earth Syst., 12, e2019MS001978, https://doi.org/10.1029/2019MS001978, 2020.

Buchard, V., da Silva, A. M., Randles, C. A., Colarco, P., Ferrare, R., Hair, J., Hostetler, C., Tackett, J., and Winker, D.: Evaluation of the surface $PM_{2.5}$ in Version 1 of the NASA MERRA Aerosol Reanalysis over the United States, Atmos. Environ., 125, 100-111, https://doi.org/10.1016/j.atmosenv.2015.11.004, 2016.

Bürki, C., Reggente, M., Dillner, A. M., Hand, J. L., Shaw, S. L., and Takahama, S.: Analysis of functional groups in atmospheric aerosols by infrared spectroscopy: method development for probabilistic modeling of organic carbon and organic matter concentrations, Atmos. Meas. Tech., 13, 1517-1538, https://doi.org/10.5194/amt-13-1517-2020, 2020.

Carslaw, K. S., Lee, L. A., Reddington, C. L., Pringle, K. J., Rap, A., Forster, P. M., Mann, G. W., Spracklen, D. V., Woodhouse, M. T., Regayre, L. A., and Pierce, J. R.: Large contribution of natural aerosols to uncertainty in indirect forcing, Nature, 503, 67-71, https://doi.org/10.1038/nature12674, 2013.

Chen, D., Liao, H., Yang, Y., Chen, L., Zhao, D., and Ding, D.: Simulated impacts of vertical distributions of black carbon aerosol on meteorology and $PM_{2.5}$ concentrations in Beijing during severe haze events,

Atmos. Chem. Phys., 22, 1825-1844, https://doi.org/10.5194/acp-22-1825-2022, 2022.

Chen, Y., Li, J., Lee, W., Diner, D., Garay, M., Jiang, J., Wang, Y., Yu, J., and Kalashnikova, O.: Evaluation of sea salt aerosols in climate systems: global climate modeling and observation-based analyses, Environ. Res. Lett., 15, 034047, https://doi.org/10.1088/1748-9326/ab751c, 2020.

Chen, Z., Liu, J. F., Tao, W., and Tao, S.: Spatiotemporal distribution and source attribution of SOA in China, Huan Jing Ke Xue, 37, 2815-2822, https://doi.org/10.13227/j.hjkx.2016.08.001, 2016.

Cherian, R. and Quaas, J.: Trends in AOD, Clouds, and Cloud Radiative Effects in Satellite Data and CMIP5 and CMIP6 Model Simulations Over Aerosol Source Regions, Geophys. Res. Lett., 47, e2020GL087132, https://doi.org/10.1029/2020GL087132, 2020.

de Leeuw, G., Fan, C., Li, Z., Dong, J., Li, Y., Ou, Y., and Zhu, S.: Spatiotemporal variation and provincial scale differences of the AOD across China during 2000–2021, Atmos. Pollut. Res., 13, 101359, https://doi.org/10.1016/j.apr.2022.101359, 2022.

Digby, R., Gillett, N., Monahan, A., von Salzen, K., Gkikas, A., Song, Q., and Zhang, Z.: How well do Earth system models reproduce the observed aerosol response to rapid emission reductions? A COVID-19 case study, Atmos. Chem. Phys., 24, 2077-2097, https://doi.org/10.5194/acp-24-2077-2024, 2024.

Dunne, J. P., Horowitz, L. W., Adcroft, A. J., Ginoux, P., Held, I. M., John, J. G., Krasting, J. P., Malyshev, S., Naik, V., Paulot, F., Shevliakova, E., Stock, C. A., Zadeh, N., Balaji, V., Blanton, C., Dunne, K. A., Dupuis, C., Durachta, J., Dussin, R., Gauthier, P. P. G., Griffies, S. M., Guo, H., Hallberg, R. W., Harrison, M., He, J., Hurlin, W., McHugh, C., Menzel, R., Milly, P. C. D., Nikonov, S., Paynter, D. J., Ploshay, J., Radhakrishnan, A., Rand, K., Reichl, B. G., Robinson, T., Schwarzkopf, D. M., Sentman, L. T., Underwood, S., Vahlenkamp, H., Winton, M., Wittenberg, A. T., Wyman, B., Zeng, Y., and Zhao, M.: The GFDL Earth System Model Version 4.1 (GFDL-ESM 4.1): Overall Coupled Model Description and Simulation Characteristics, J. Adv. Model. Earth Syst., 12, e2019MS002015, https://doi.org/10.1029/2019MS002015, 2020.

Evan, A. T., Flamant, C., Gaetani, M., and Guichard, F.: The past, present and future of African dust, Nature, 531, 493-495, https://doi.org/10.1038/nature17149 2016.

Eyring, V., Bony, S., Meehl, G. A., Senior, C. A., Stevens, B., Stouffer, R. J., and Taylor, K. E.: Overview of the Coupled Model Intercomparison Project Phase 6 (CMIP6) experimental design and organization, Geosci. Model Dev., 9, 1937-1958, https://doi.org/10.5194/gmd-9-1937-2016, 2016.

Fan, T., Liu, X., Wu, C., Zhang, Q., Zhao, C., Yang, X., and Li, Y.: Comparison of the Anthropogenic Emission Inventory for CMIP6 Models with a Country-Level Inventory over China and the Simulations of the Aerosol Properties, Adv. Atmos. Sci., 39, 80-96, https://doi.org/10.1007/s00376-021-1119-6, 2022.

Fan, T., Zhao, C., Dong, X., Liu, X., Yang, X., Zhang, F., Shi, C., Wang, Y., and Wu, F.: Quantify contribution of aerosol errors to cloud fraction biases in CMIP5 Atmospheric Model Intercomparison Project simulations, Int. J. Climatol., 38, 3140-3156, https://doi.org/10.1002/joc.5490, 2018a.

Fan, T., Liu, X., Ma, P. L., Zhang, Q., Li, Z., Jiang, Y., Zhang, F., Zhao, C., Yang, X., Wu, F., and Wang,

548 Y.: Emission or atmospheric processes? An attempt to attribute the source of large bias of aerosols in
549 eastern China simulated by global climate models, Atmos. Chem. Phys., 18, 1395-1417,
550 https://doi.org/10.5194/acp-18-1395-2018, 2018b.

551 Feng, L., Smith, S. J., Braun, C., Crippa, M., Gidden, M. J., Hoesly, R., Klimont, Z., van Marle, M., van
552 den Berg, M., and van der Werf, G. R.: The generation of gridded emissions data for CMIP6, Geosci.
553 Model Dev., 13, 461-482, https://doi.org/10.5194/gmd-13-461-2020, 2020.

554 Fountoukis, C. and Nenes, A.: ISORROPIA II: a computationally efficient thermodynamic equilibrium
555 model for K+-Ca2+-Mg2+-NH4+-Na+-SO42--NO3--Cl--H2O aerosols, Atmos. Chem. Phys., 7, 4639-
556 4659, https://doi.org/10.5194/acp-7-4639-2007, 2007.

557 Geng, G., Xiao, Q., Liu, S., Liu, X., Cheng, J., Zheng, Y., Xue, T., Tong, D., Zheng, B., Peng, Y., Huang,
558 X., He, K., and Zhang, Q.: Tracking Air Pollution in China: Near Real-Time PM2.5 Retrievals from
559 Multisource Data Fusion, Environ. Sci. Technol., 55, 12106-12115,
560 https://doi.org/10.1021/acs.est.1c01863, 2021.

561 Hammer, M. S., van Donkelaar, A., Li, C., Lyapustin, A., Sayer, A. M., Hsu, N. C., Levy, R. C., Garay,
562 M. J., Kalashnikova, O. V., Kahn, R. A., Brauer, M., Apte, J. S., Henze, D. K., Zhang, L., Zhang, Q.,
563 Ford, B., Pierce, J. R., and Martin, R. V.: Global Estimates and Long-Term Trends of Fine Particulate
564 Matter Concentrations (1998–2018), Environ. Sci. Technol., 54, 7879-7890,
565 https://doi.org/10.1021/acs.est.0c01764, 2020.

566 Hoesly, R. M., Smith, S. J., Feng, L., Klimont, Z., Janssens-Maenhout, G., Pitkanen, T., Seibert, J. J., Vu,
567 L., Andres, R. J., Bolt, R. M., Bond, T. C., Dawidowski, L., Kholod, N., Kurokawa, J. I., Li, M., Liu, L.,
568 Lu, Z., Moura, M. C. P., O'Rourke, P. R., and Zhang, Q.: Historical (1750–2014) anthropogenic emissions
569 of reactive gases and aerosols from the Community Emissions Data System (CEDS), Geosci. Model Dev.,
570 11, 369-408, https://doi.org/10.5194/gmd-11-369-2018, 2018.

571 Huang, Y., Shen, H., Chen, Y., Zhong, Q., Chen, H., Wang, R., Shen, G., Liu, J., Li, B., and Tao, S.:
572 Global organic carbon emissions from primary sources from 1960 to 2009, Atmos. Environ., 122, 505-
573 512, https://doi.org/10.1016/j.atmosenv.2015.10.017, 2015.

574 Jacob, D. J.: Heterogeneous chemistry and tropospheric ozone, Atmos. Environ., 34, 2131-2159,
575 https://doi.org/10.1016/S1352-2310(99)00462-8, 2000.

576 Li, K., Jacob, D. J., Liao, H., Zhu, J., Shah, V., Shen, L., Bates, K. H., Zhang, Q., and Zhai, S.: A two-
577 pollutant strategy for improving ozone and particulate air quality in China, Nat. Geosci., 12, 906-910,
578 https://doi.org/10.1038/s41561-019-0464-x, 2019.

579 Li, R., Ma, X., Xiong, F., Jia, H., Sha, T., and Tian, R.: Comparisons and evaluation of aerosol burden
580 and optical depth in CMIP5 simulations over East Asia, J. Atmos. Solar-Terr. Phys., 206, 105315,
581 https://doi.org/10.1016/j.jastp.2020.105315, 2020.

582 Li, X., Liu, Y., Wang, M., Jiang, Y., and Dong, X.: Assessment of the Coupled Model Intercomparison
583 Project phase 6 (CMIP6) Model performance in simulating the spatial-temporal variation of aerosol
584 optical depth over Eastern Central China, Atmos. Res., 261, 105747,

https://doi.org/10.1016/j.atmosres.2021.105747, 2021.

Lin, J., Liu, Z., Zhang, Q., Liu, H., Mao, J., and Zhuang, G.: Modeling uncertainties for tropospheric nitrogen dioxide columns affecting satellite-based inverse modeling of nitrogen oxides emissions, Atmos. Chem. Phys., 12, 12255-12275, https://doi.org/10.5194/acp-12-12255-2012, 2012.

Lin, J., Tong, D., Davis, S., Ni, R., Tan, X., Pan, D., Zhao, H., Lu, Z., Streets, D., Feng, T., Zhang, Q., Yan, Y., Hu, Y., Li, J., Liu, Z., Jiang, X., Geng, G., He, K., Huang, Y., and Guan, D.: Global climate forcing of aerosols embodied in international trade, Nat. Geosci., 9, 790-794, https://doi.org/10.1038/ngeo2798, 2016.

~~Lin, J. T., Liu, Z., Zhang, Q., Liu, H., Mao, J., and Zhuang, G.: Modeling uncertainties for tropospheric nitrogen dioxide columns affecting satellite-based inverse modeling of nitrogen oxides emissions, Atmos. Chem. Phys., 12, 12255-12275, https://doi.org/10.5194/acp-12-12255-2012, 2012.~~

Liu, R. ~~J~~. and Liao, H.: Assessment of aerosol effective radiative forcing and surface air temperature response over eastern China in CMIP5 models, Atmos. Oceanic Sci. Lett., 10, 228-234, https://doi.org/10.1080/16742834.2017.1301188, 2017.

Ma, X., Yan, P., Zhao, T., Jia, X., Jiao, J., Ma, Q., Wu, D., Shu, Z., Sun, X., and Habtemicheal, B. A.: Evaluations of Surface PM10 Concentration and Chemical Compositions in MERRA-2 Aerosol Reanalysis over Central and Eastern China, Remote Sens., 13, 1317, https://doi.org/10.3390/rs13071317, 2021.

Mahesh, B., Rama, B. V., Spandana, B., Sarma, M. S. S. R. K. N., Niranjan, K., and Sreekanth, V.: Evaluation of MERRAero $PM_{2.5}$ over Indian cities, Adv. Space Res., 64, 328-334, https://doi.org/10.1016/j.asr.2019.04.026, 2019.

McDuffie, E. E., Smith, S. J., O'Rourke, P., Tibrewal, K., Venkataraman, C., Marais, E. A., Zheng, B., Crippa, M., Brauer, M., and Martin, R. V.: A global anthropogenic emission inventory of atmospheric pollutants from sector- and fuel-specific sources (1970–2017): an application of the Community Emissions Data System (CEDS), Earth Syst. Sci. Data, 12, 3413-3442, https://doi.org/10.5194/essd-12-3413-2020, 2020.

Metzger, S., Dentener, F., Pandis, S., and Lelieveld, J.: Gas/aerosol partitioning: 1. A computationally efficient model, J. Geophys. Res. Atmos., 107, ACH 16-11-ACH 16-24, https://doi.org/10.1029/2001JD001102, 2002.

Michou, M., Nabat, P., Saint-Martin, D., Bock, J., Decharme, B., Mallet, M., Roehrig, R., Séférian, R., Sénési, S., and Voldoire, A.: Present-Day and Historical Aerosol and Ozone Characteristics in CNRM CMIP6 Simulations, J. Adv. Model. Earth Syst., 12, e2019MS001816, https://doi.org/10.1029/2019MS001816, 2020.

Mortier, A., Gliß, J., Schulz, M., Aas, W., Andrews, E., Bian, H., Chin, M., Ginoux, P., Hand, J., Holben, B., Zhang, H., Kipling, Z., Kirkevåg, A., Laj, P., Lurton, T., Myhre, G., Neubauer, D., Olivié, D., von Salzen, K., Skeie, R. B., Takemura, T., and Tilmes, S.: Evaluation of climate model aerosol trends with ground-based observations over the last 2 decades – an AeroCom and CMIP6 analysis, Atmos. Chem.

622 Phys., 20, 13355-13378, https://doi.org/10.5194/acp-20-13355-2020, 2020.

623 Mulcahy, J. P., Johnson, C., Jones, C. G., Povey, A. C., Scott, C. E., Sellar, A., Turnock, S. T., Woodhouse,
624 M. T., Abraham, N. L., Andrews, M. B., Bellouin, N., Browse, J., Carslaw, K. S., Dalvi, M., Folberth, G.
625 A., Glover, M., Grosvenor, D. P., Hardacre, C., Hill, R., Johnson, B., Jones, A., Kipling, Z., Mann, G.,
626 Mollard, J., O'Connor, F. M., Palmiéri, J., Reddington, C., Rumbold, S. T., Richardson, M., Schutgens,
627 N. A. J., Stier, P., Stringer, M., Tang, Y., Walton, J., Woodward, S., and Yool, A.: Description and
628 evaluation of aerosol in UKESM1 and HadGEM3-GC3.1 CMIP6 historical simulations, Geosci. Model
629 Dev., 13, 6383-6423, https://doi.org/10.5194/gmd-13-6383-2020, 2020.

630 Park, H., Chung, C. E., Ekman, A. M. L., and Choi, J.-O.: Evaluation of ACCMIP simulated fine-mode
631 AOD and its implication for aerosol direct forcing, Asia Pac. J. Atmos. Sci., 50, 377-390,
632 https://doi.org/10.1007/s13143-014-0025-6, 2014.

633 Paulot, F., Paynter, D., Ginoux, P., Naik, V., and Horowitz, L. W.: Changes in the aerosol direct radiative
634 forcing from 2001 to 2015: observational constraints and regional mechanisms, Atmos. Chem. Phys., 18,
635 13265-13281, https://doi.org/10.5194/acp-18-13265-2018, 2018.

636 Paulot, F., Ginoux, P., Cooke, W. F., Donner, L. J., Fan, S., Lin, M. Y., Mao, J., Naik, V., and Horowitz,
637 L. W.: Sensitivity of nitrate aerosols to ammonia emissions and to nitrate chemistry: implications for
638 present and future nitrate optical depth, Atmos. Chem. Phys., 16, 1459-1477, https://doi.org/10.5194/acp-
639 16-1459-2016, 2016.

640 Pu, B. and Ginoux, P.: How reliable are CMIP5 models in simulating dust optical depth?, Atmos. Chem.
641 Phys., 18, 12491-12510, https://doi.org/10.5194/acp-18-12491-2018, 2018.

642 Seinfeld, J. H., Bretherton, C., Carslaw, K. S., Coe, H., DeMott, P. J., Dunlea, E. J., Feingold, G., Ghan,
643 S., Guenther, A. B., Kahn, R., Kraucunas, I., Kreidenweis, S. M., Molina, M. J., Nenes, A., Penner, J. E.,
644 Prather, K. A., Ramanathan, V., Ramaswamy, V., Rasch, P. J., Ravishankara, A. R., Rosenfeld, D.,
645 Stephens, G., and Wood, R.: Improving our fundamental understanding of the role of aerosol−cloud
646 interactions in the climate system, P. Natl. Acad. Sci. USA, 113, 5781-5790,
647 https://doi.org/10.1073/pnas.1514043113, 2016.

648 Shim, S., Sung, H., Kwon, S., Kim, J., Lee, J., Sun, M., Song, J., Ha, J., Byun, Y., Kim, Y., Turnock, S.
649 T., Stevenson, D. S., Allen, R. J., O'Connor, F. M., Teixeira, J. C., Williams, J., Johnson, B., Keeble, J.,
650 Mulcahy, J., and Zeng, G.: Regional Features of Long-Term Exposure to $PM_{2.5}$ Air Quality over Asia
651 under SSP Scenarios Based on CMIP6 Models, Int. J. Environ. Res. Public Health, 18, 6817,
652 https://doi.org/10.3390/ijerph18136817, 2021.

653 Sockol, A. and Small Griswold, J. D.: Intercomparison between CMIP5 model and MODIS satellite-
654 retrieved data of aerosol optical depth, cloud fraction, and cloud-aerosol interactions, Earth Space Sci.,
655 4, 485-505, https://doi.org/10.1002/2017EA000288, 2017.

656 Song, H., Zhang, K., Piao, S., and Wan, S.: Spatial and temporal variations of spring dust emissions in
657 northern China over the last 30 years, Atmos. Environ., 126, 117-127,
658 https://doi.org/10.1016/j.atmosenv.2015.11.052, 2016.

659 Su, X., Wu, T., Zhang, J., Zhang, Y., Jin, J., Zhou, Q., Zhang, F., Liu, Y., Zhou, Y., Zhang, L., Turnock,
660 S. T., and Furtado, K.: Present-Day $PM_{2.5}$ over Asia: Simulation and Uncertainty in CMIP6 ESMs, J.
661 Meteorol. Res., 36, 429-449, https://doi.org/10.1007/s13351-022-1202-7, 2022.

662 Tang, Z., Tian, J., Zhang, Y., Zhang, X., Zhang, J., Ma, N., Li, X., and Song, P.: Anthropogenic aerosols
663 dominated the decreased solar radiation in eastern China over the last five decades, J. Clean. Prod., 380,
664 135150, https://doi.org/10.1016/j.jclepro.2022.135150, 2022.

665 Tao, S., Ru, M. Y., Du, W., Zhu, X., Zhong, Q. R., Li, B. G., Shen, G. F., Pan, X. L., Meng, W. J., Chen,
666 Y. L., Shen, H. Z., Lin, N., Su, S., Zhuo, S. J., Huang, T. B., Xu, Y., Yun, X., Liu, J. F., Wang, X. L., Liu,
667 W. X., Cheng, H. F., and Zhu, D. Q.: Quantifying the rural residential energy transition in China from
668 1992 to 2012 through a representative national survey, Nat. Energy, 3, 567-573,
669 https://doi.org/10.1038/s41560-018-0158-4, 2018.

670 Tegen, I., Neubauer, D., Ferrachat, S., Siegenthaler-Le Drian, C., Bey, I., Schutgens, N., Stier, P., Watson-
671 Parris, D., Stanelle, T., Schmidt, H., Rast, S., Kokkola, H., Schultz, M., Schroeder, S., Daskalakis, N.,
672 Barthel, S., Heinold, B., and Lohmann, U.: The global aerosol–climate model ECHAM6.3–HAM2.3 –
673 Part 1: Aerosol evaluation, Geosci. Model Dev., 12, 1643-1677, https://doi.org/10.5194/gmd-12-1643-
674 2019, 2019.

675 Turnock, S. T., Allen, R. J., Andrews, M., Bauer, S. E., Deushi, M., Emmons, L., Good, P., Horowitz, L.,
676 John, J. G., Michou, M., Nabat, P., Naik, V., Neubauer, D., O'Connor, F. M., Olivié, D., Oshima, N.,
677 Schulz, M., Sellar, A., Shim, S., Takemura, T., Tilmes, S., Tsigaridis, K., Wu, T., and Zhang, J.: Historical
678 and future changes in air pollutants from CMIP6 models, Atmos. Chem. Phys., 20, 14547-14579,
679 https://doi.org/10.5194/acp-20-14547-2020, 2020.

680 van Donkelaar, A., Martin, R. V., Li, C., and Burnett, R. T.: Regional Estimates of Chemical Composition
681 of Fine Particulate Matter Using a Combined Geoscience-Statistical Method with Information from
682 Satellites, Models, and Monitors, Environ. Sci. Technol., 53, 2595-2611,
683 https://doi.org/10.1021/acs.est.8b06392, 2019.

684 van Donkelaar, A., Martin, R. V., Brauer, M., Hsu, N. C., Kahn, R. A., Levy, R. C., Lyapustin, A., Sayer,
685 A. M., and Winker, D. M.: Global Estimates of Fine Particulate Matter using a Combined Geophysical-
686 Statistical Method with Information from Satellites, Models, and Monitors, Environ. Sci. Technol., 50,
687 3762-3772, https://doi.org/10.1021/acs.est.5b05833, 2016.

688 van Donkelaar, A., Hammer, M. S., Bindle, L., Brauer, M., Brook, J. R., Garay, M. J., Hsu, N. C.,
689 Kalashnikova, O. V., Kahn, R. A., Lee, C., Levy, R. C., Lyapustin, A., Sayer, A. M., and Martin, R. V.:
690 Monthly Global Estimates of Fine Particulate Matter and Their Uncertainty, Environ. Sci. Technol., 55,
691 15287-15300, https://doi.org/10.1021/acs.est.1c05309, 2021.

692 van Noije, T., Bergman, T., Le Sager, P., O'Donnell, D., Makkonen, R., Gonçalves-Ageitos, M., Döscher,
693 R., Fladrich, U., von Hardenberg, J., Keskinen, J. P., Korhonen, H., Laakso, A., Myriokefalitakis, S.,
694 Ollinaho, P., Pérez García-Pando, C., Reerink, T., Schrödner, R., Wyser, K., and Yang, S.: EC-Earth3-
695 AerChem: a global climate model with interactive aerosols and atmospheric chemistry participating in
696 CMIP6, Geosci. Model Dev., 14, 5637-5668, https://doi.org/10.5194/gmd-14-5637-2021, 2021.

Wang, C., Wang, Z., Lei, Y., Zhang, H., Che, H., and Zhang, X.: Differences in East Asian summer monsoon responses to Asian aerosol forcing under different emission inventories, Adv. Clim. Change Res., 13, 309-322, https://doi.org/10.1016/j.accre.2022.02.008, 2022.

Wang, R., Tao, S., Shen, H., Huang, Y., Chen, H., Balkanski, Y., Boucher, O., Ciais, P., Shen, G., Li, W., Zhang, Y., Chen, Y., Lin, N., Su, S., Li, B., Liu, J., and Liu, W.: Trend in Global Black Carbon Emissions from 1960 to 2007, Environ. Sci. Technol., 48, 6780-6787, https://doi.org/10.1021/es5021422, 2014.

Wang, S., Yu, Y., Zhang, X., Lu, H., Zhang, X., and Xu, Z.: Weakened dust activity over China and Mongolia from 2001 to 2020 associated with climate change and land-use management, Environ. Res. Lett., 16, https://doi.org/10.1088/1748-9326/ac3b79, 2021a.

Wang, Z., Lin, L., Xu, Y., Che, H., Zhang, X., Zhang, H., Dong, W., Wang, C., Gui, K., and Xie, B.: Incorrect Asian aerosols affecting the attribution and projection of regional climate change in CMIP6 models, NPJ Clim. Atmos. Sci., 4, 2, https://doi.org/10.1038/s41612-020-00159-2, ~~2021~~2021b.

Wilcox, L. J., Allen, R. J., Samset, B. H., Bollasina, M. A., Griffiths, P. T., Keeble, J. M., Lund, M. T., Makkonen, R., Merikanto, J., O'Donnell, D., Paynter, D. J., Persad, G. G., Rumbold, S. T., Takemura, T., Tsigaridis, K., Undorf, S., and Westervelt, D. M.: The Regional Aerosol Model Intercomparison Project (RAMIP), Geosci. Model Dev. Discuss., 2022, 1-40, https://doi.org/10.5194/gmd-2022-249, 2022.

World Health Organization: WHO global air quality guidelines: particulate matter ($PM_{2.5}$ and PM_{10}), ozone, nitrogen dioxide, sulfur dioxide and carbon monoxide, World Health Organization, https://apps.who.int/iris/handle/10665/345329, 2021.

Wu, J., Shi, Y., and Xu, Y.: Evaluation and Projection of Surface Wind Speed Over China Based on CMIP6 GCMs, J. Geophys. Res. Atmos., 125, e2020JD033611, https://doi.org/10.1029/2020JD033611, ~~2020~~2020a.

Wu, T., Zhang, F., Zhang, J., Jie, W., Zhang, Y., Wu, F., Li, L., Yan, J., Liu, X., Lu, X., Tan, H., Zhang, L., Wang, J., and Hu, A.: Beijing Climate Center Earth System Model version 1 (BCC-ESM1): model description and evaluation of aerosol simulations, Geosci. Model Dev., 13, 977-1005, https://doi.org/10.5194/gmd-13-977-2020, 2020b.

Wu, T., Lu, Y., Fang, Y., Xin, X., Li, L., Li, W., Jie, W., Zhang, J., Liu, Y., Zhang, L., Zhang, F., Zhang, Y., Wu, F., Li, J., Chu, M., Wang, Z., Shi, X., Liu, X., Wei, M., Huang, A., Zhang, Y., and Liu, X.: The Beijing Climate Center Climate System Model (BCC-CSM): the main progress from CMIP5 to CMIP6, Geosci. Model Dev., 12, 1573-1600, https://doi.org/10.5194/gmd-12-1573-2019, 2019.

Xu, Y., Wu, J., and Han, Z.: Evaluation and Projection of Surface $PM_{2.5}$ and Its Exposure on Population in Asia Based on the CMIP6 GCMs, Int. J. Environ. Res. Public Health, 19, 12092, https://doi.org/10.3390/ijerph191912092, 2022.

Yang, X., Zhou, B., Xu, Y., and Han, Z.: CMIP6 Evaluation and Projection of Temperature and Precipitation over China, Adv. Atmos. Sci., 38, 817-830, https://doi.org/10.1007/s00376-021-0351-4, 2021.

Yue, M., Wang, M., Guo, J., Zhang, H., Dong, X., and Liu, Y.: Long-Term Trend Comparison of Planetary Boundary Layer Height in Observations and CMIP6 Models over China, J. Clim., 34, 8237-8256, https://doi.org/10.1175/JCLI-D-20-1000.1, 2021.

Zhai, S., Jacob, D. J., Wang, X., Shen, L., Li, K., Zhang, Y., Gui, K., Zhao, T., and Liao, H.: Fine particulate matter ($PM_{2.5}$) trends in China, 2013–2018: separating contributions from anthropogenic emissions and meteorology, Atmos. Chem. Phys., 19, 11031-11041, https://doi.org/10.5194/acp-19-11031-2019, 2019.

Zhai, S., Jacob, D. J., Wang, X., Liu, Z., Wen, T., Shah, V., Li, K., Moch, J. M., Bates, K. H., Song, S., Shen, L., Zhang, Y., Luo, G., Yu, F., Sun, Y., Wang, L., Qi, M., Tao, J., Gui, K., Xu, H., Zhang, Q., Zhao, T., Wang, Y., Lee, H. C., Choi, H., and Liao, H.: Control of particulate nitrate air pollution in China, Nat. Geosci., 14, 389-395, https://doi.org/10.1038/s41561-021-00726-z, 2021.

Zhang, L., Li, J., Jiang, Z., Dong, Y., Ying, T., and Zhang, Z.: Clear-Sky Direct Aerosol Radiative Forcing Uncertainty Associated with Aerosol Optical Properties Based on CMIP6 Models, J. Climate, 35, 3007-3019, https://doi.org/10.1175/JCLI-D-21-0479.1, ~~2022~~2022a.

Zhang, Q., Jiang, X., Tong, D., Davis, S. J., Zhao, H., Geng, G., Feng, T., Zheng, B., Lu, Z., Streets, D. G., Ni, R., Brauer, M., van Donkelaar, A., Martin, R. V., Huo, H., Liu, Z., Pan, D., Kan, H., Yan, Y., Lin, J., He, K., and Guan, D.: Transboundary health impacts of transported global air pollution and international trade, Nature, 543, 705-709, https://doi.org/10.1038/nature21712, 2017.

Zhang, X., Hua, L., and Jiang, D.: Assessment of CMIP6 model performance for temperature and precipitation in Xinjiang, China, Atmos. Oceanic Sci. Lett., 15, 100128, https://doi.org/10.1016/j.aosl.2021.100128, 2022b.

Zhao, A., Ryder, C. L., and Wilcox, L. J.: How well do the CMIP6 models simulate dust aerosols?, Atmos. Chem. Phys., 22, 2095-2119, https://doi.org/10.5194/acp-22-2095-2022, 2022.

Zheng, B., Tong, D., Li, M., Liu, F., Hong, C., Geng, G., Li, H., Li, X., Peng, L., Qi, J., Yan, L., Zhang, Y., Zhao, H., Zheng, Y., He, K., and Zhang, Q.: Trends in China's anthropogenic emissions since 2010 as the consequence of clean air actions, Atmos. Chem. Phys., 18, 14095-14111, ~~10.5194/acp-18-14095-2018,~~https://doi.org/10.5194/acp-18-14095-2018, 2018.

Zhu, H., Jiang, Z., Li, J., Li, W., Sun, C., and Li, L.: Does CMIP6 Inspire More Confidence in Simulating Climate Extremes over China?, Adv. Atmos. Sci., 37, 1119-1132, https://doi.org/10.1007/s00376-020-9289-1, 2020.

Zhu, Y. and Yang, S.: Evaluation of CMIP6 for historical temperature and precipitation over the Tibetan Plateau and its comparison with CMIP5, Adv. Clim. Chang. Res., 11, 239-251, https://doi.org/10.1016/j.accre.2020.08.001, 2020.

–

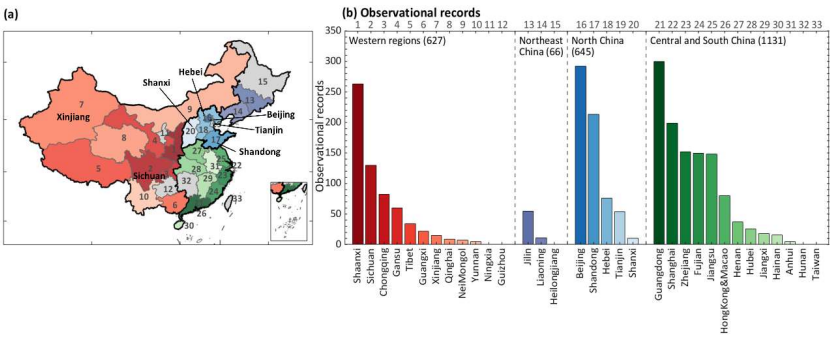

Figure 1. Observational records of $PM_{2.5}$ components during 2000–2014 collected from the literature. (a) The map depicts individual provinces in four regions, including the western regions in red colors, Northeast China in purple, North China in blue, and Central and South China in green. The provinces without observational records are in gray. The number denotes each province. (b) Provincial observation records in China. The number in the upper x-axis and the color in each bar match the province in (a).

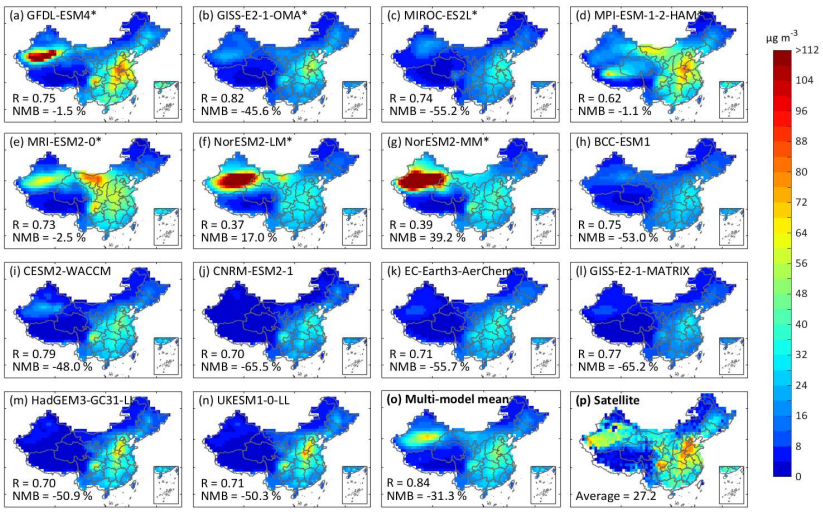

Figure 2. Multi-year mean annual average near-surface total $PM_{2.5}$ concentrations over China during 2000–2014. (a-g) Model outputted $PM_{2.5}$ concentrations in seven models. (h-n) Calculated $PM_{2.5}$ concentrations in the other seven models according to Eq. 1. (o) Multi-model mean. (p) Satellite-based total $PM_{2.5}$ dataset. R stands for spatial correlation, and NMB stands for normalized mean bias.

Formatted: Justified

Formatted: Font: Not Bold

Formatted: Font: Not Bold

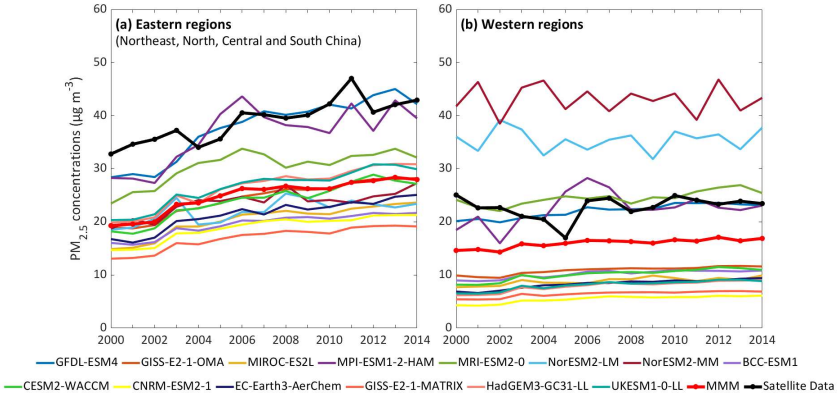

Figure 3. Time series of annual mean regional average total $PM_{2.5}$ concentrations. (a) Over the eastern regions (including Northeast China, North China, and Central and South China). (b) Over the western regions. The bold black lines denote satellite-based $PM_{2.5}$ concentrations, and the bold red lines denote multi-model mean (MMM) concentrations.

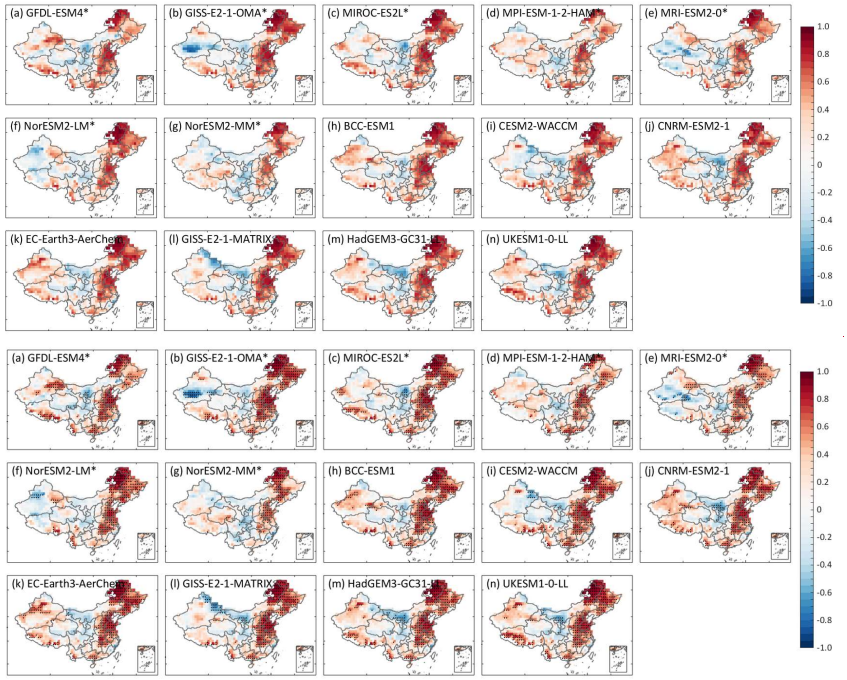

Figure 4. Spatial distribution of correlation coefficients between modeled and satellite-based data for interannual variations of annual mean total $PM_{2.5}$ concentrations ~~over~~during 2000–2014. Black dots indicate a significance level

of 0.05.

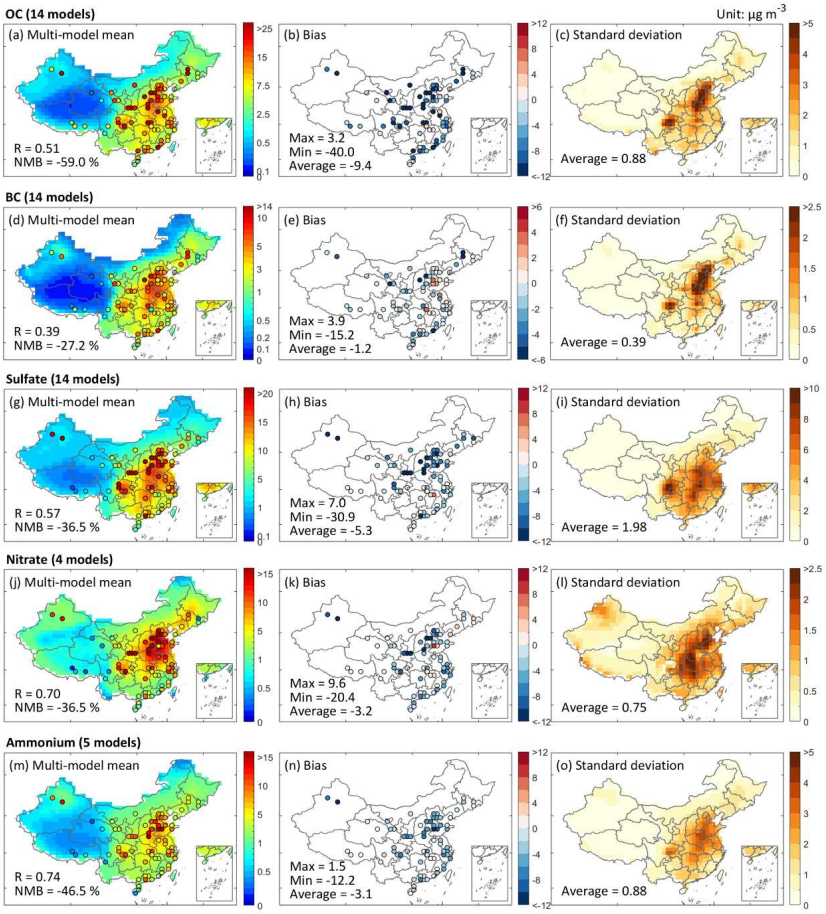

Figure 5. ~~The spatial~~Spatial distribution of multi-year averages of modeled $PM_{2.5}$ components during 2000–2014. (First column) The multi-model mean $PM_{2.5}$ component concentrations, overlaid with average ground-based observations in filled circles. (Second column) The bias of multi-model mean concentrations. (Third column) The standard deviation of $PM_{2.5}$ component simulations among the CMIP6 models.

Formatted: Font: Not Bold

Formatted: Font: Not Bold

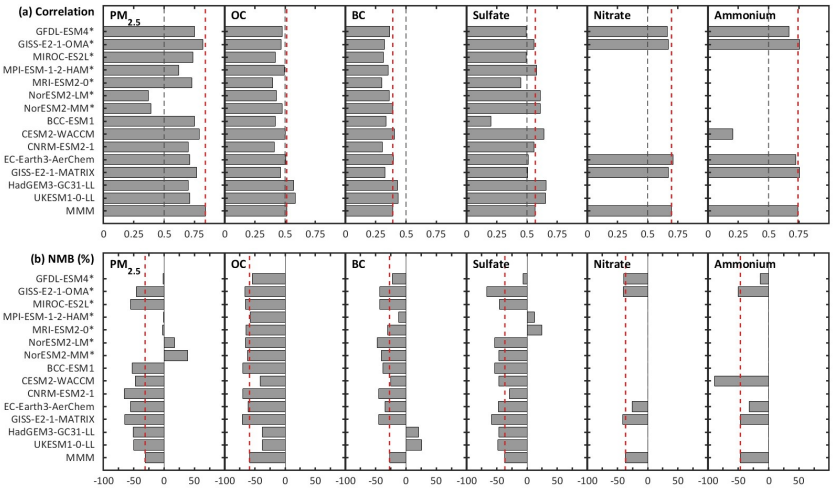

793

794 **Figure 6.** Multi-year mean spatial correlation and bias for $PM_{2.5}$ components over 2000–2014 for individual models.

795 Results for total $PM_{2.5}$ refer to the comparison against the satellite-based dataset, and those for components are

796 relative to the observations compiled from the literature. The red dotted lines denote multi-model mean (MMM).

797 The black dotted lines denote the spatial correlation coefficient value of 0.5.

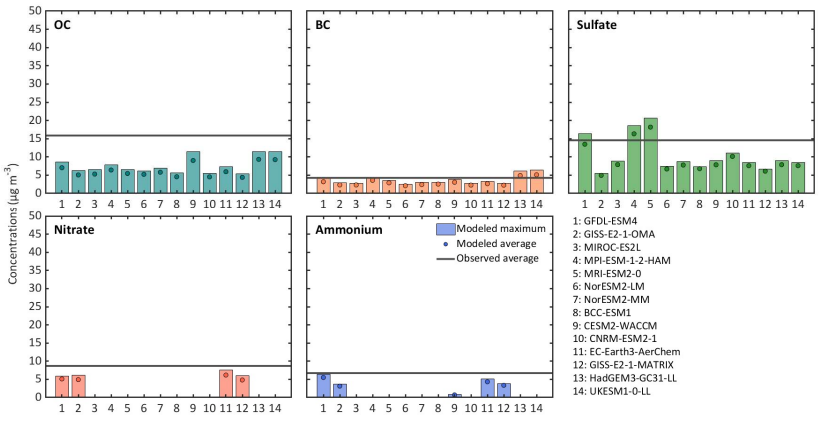

798

799 **Figure 7.** Maximum and average concentrations over 2000–2014 for simulated national mean $PM_{2.5}$ components

800 simulated by individual models. In each year, model values are sampled from grid cells with available observations.

Formatted: Font: Not Bold

Formatted: Font: Not Bold

Formatted: Font: Not Bold

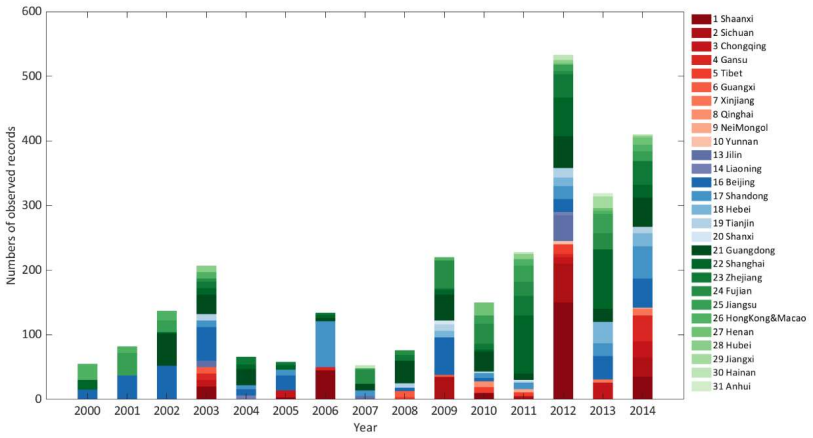

Figure S1. Provincial observed records over China during 2000–2014. The color and labeling of provinces are consistent with ~~figure~~Figure 1.

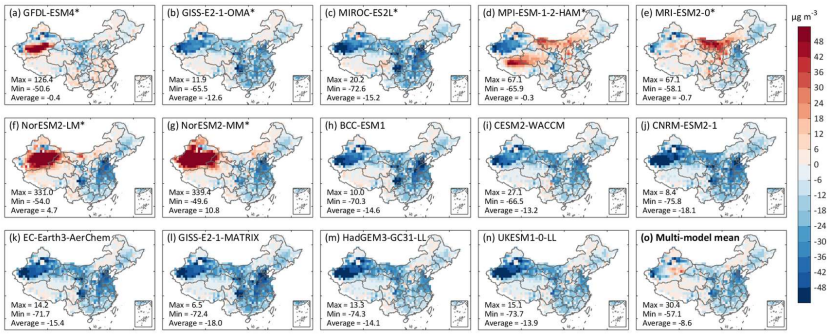

Figure S2. Spatial distribution of bias in the multi-year average of simulate-based $PM_{2.5}$ concentrations during 2000–2014 for each model.

Formatted: Font: Not Bold

Formatted: Font: Not Bold

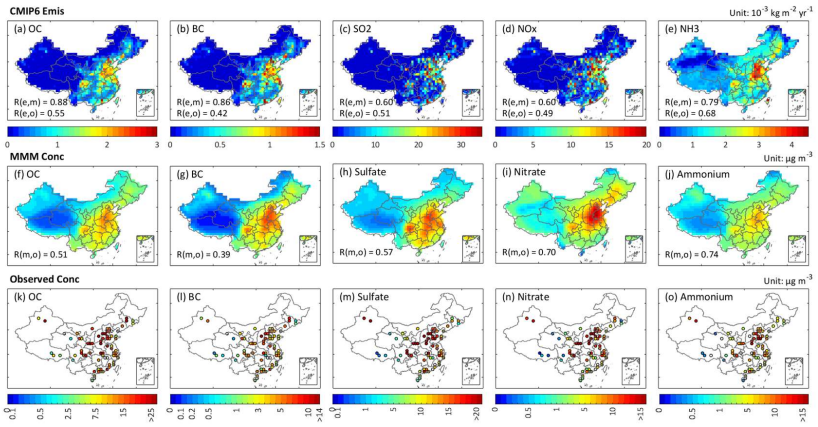

Figure S3. Multi-year average of CMIP6 emissions (a-e), multi-model mean concentrations (f-j), and observed concentrations (k-o) of air pollutants over 2000–2014. R (e, m), R (e, o), and R (m, o) denote the spatial correlation coefficients between CMIP6 emissions and multi-model mean concentrations, between CMIP6 emissions and observed concentrations, and between multi-model mean concentrations and observed concentrations.

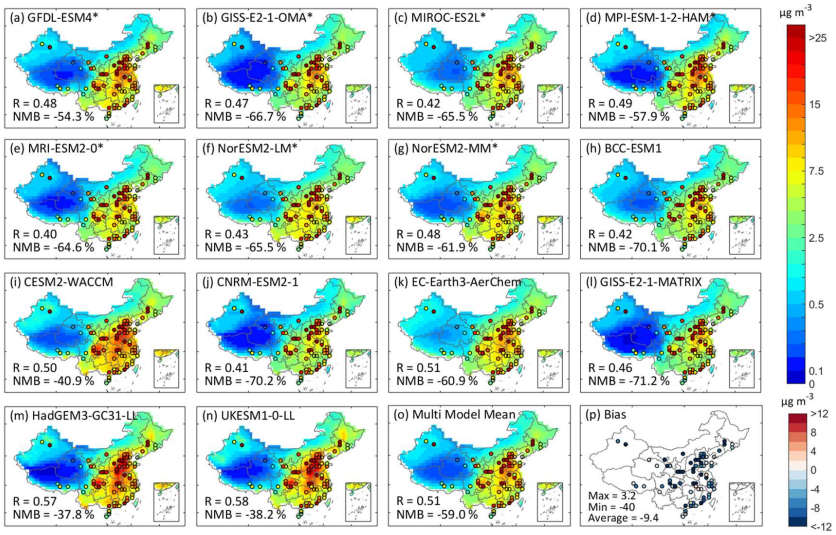

Figure S4. Multi-year mean annual average near-surface OC concentrations over China during 2000–2014. (a-n) OC in individual models overlaid with ground-based observations. (o) Multi-model mean overlaid with ground-based observations. (p) Bias in multi-model mean.

Formatted: Space After: 12 pt

Formatted: Font: Not Bold

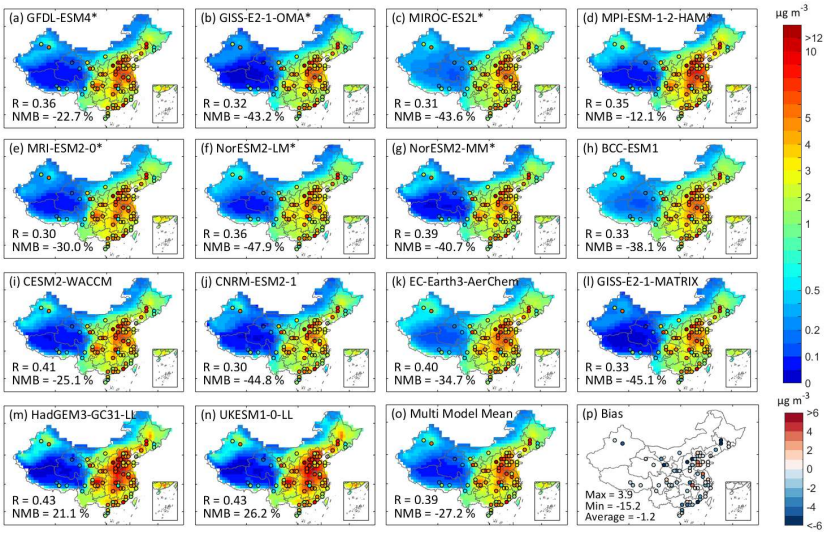

Figure S3S5. Multi-year mean annual average near-surface BC concentrations over China during 2000–2014. (a-n) BC in individual models overlaid with ground-based observations. (o) Multi-model mean overlaid with ground-based observations. (p) Bias in multi-model mean.

Formatted: Font: Not Bold

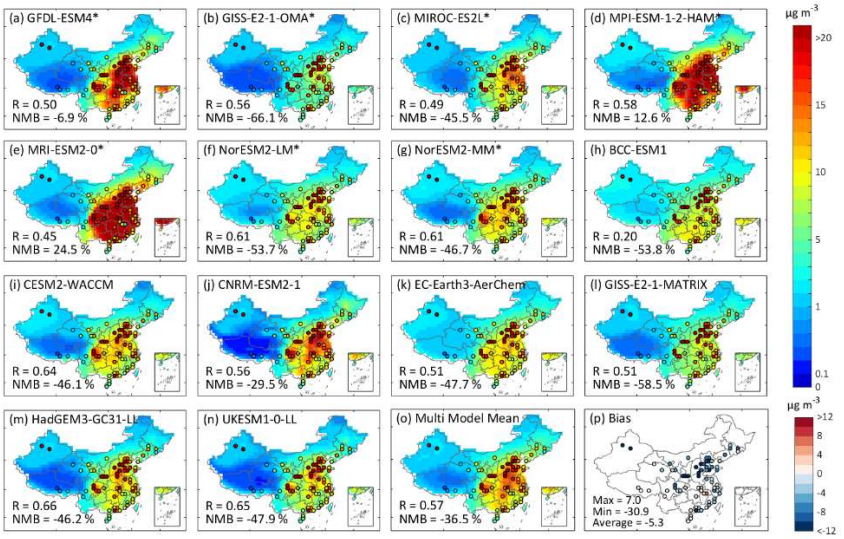

Figure S4S6. Multi-year mean annual average near-surface sulfate concentrations over China during 2000–2014. (a-n) Sulfate in individual models overlaid with ground-based observations. (o) Multi-model mean overlaid with

Formatted: Font: Not Bold

ground-based observations. (p) Bias in multi-model mean.

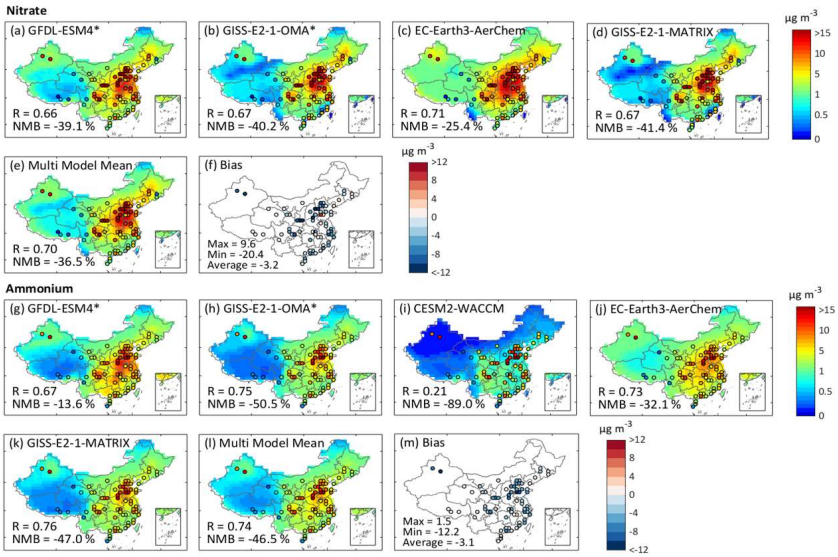

Figure S5S7. Multi-year mean annual average near-surface nitrate and ammonium concentrations over China during 2000–2014. (a-d) Nitrate and (g-k) ammonium in individual models overlaid with ground-based observations. (e, l) Multi-model mean of overlaid with ground-based observations. (f, m) Bias in multi-model mean.

Formatted: Space After: 12 pt

Formatted: Font: Not Bold

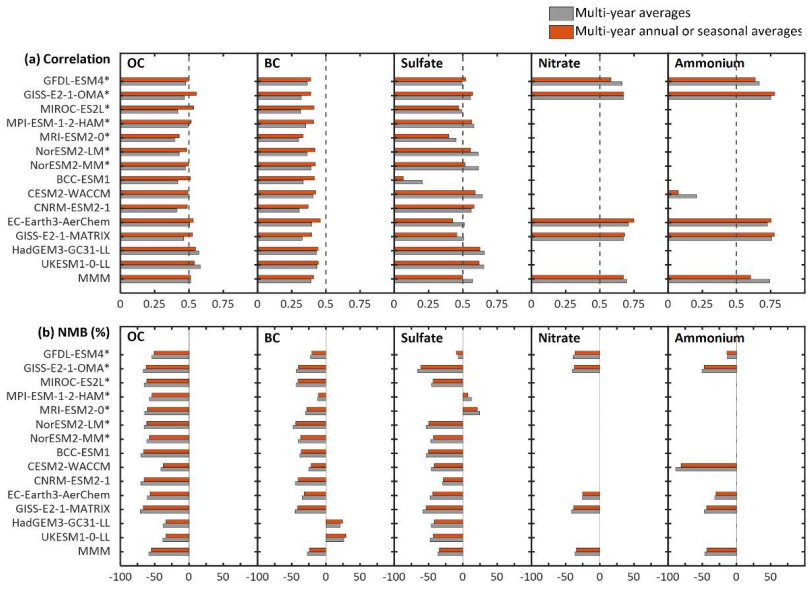

828

829 **Figure S6S8.** Spatial correlation and bias of multi-year averages (gray bar) and multi-year annual or seasonal

830 averages (red bar) of $PM_{2.5}$ components ~~over~~during 2000–2014 for individual models.

831 **Table S1.** CMIP6 models and $PM_{2.5}$ outputs.

Model	Resolution (Lat × Lon)	Number of members	OA, BC, SO_4^{2-}, SSLT, DST	NO_3^-, NH_4^+	$PM_{2.5}$	Model references and data citation
BCC-ESM1	2.813° × 2.813°	3	Y			(Wu et al., 2019; Wu et al., 2020; Zhang et al., 2018)
CESM2-WACCM	0.9° × 1.25°	3	Y	Y (No NO_3^-)		(Danabasoglu, 2019; Gettelman et al., 2019; Tilmes et al., 2019; Emmons et al., 2020)
CNRM-ESM2-1	1.4°× 1.4°	3	Y			(Séférian, 2018; Séférian et al., 2019; Michou et al., 2020)
EC-Earth3-AerChem	2° × 3°	3	Y	Y		(Van Noije et al., 2021; Döscher et al., 2022; EC-Earth Ec-Earth-Consortium, 2020)
GFDL-ESM4	1° × 1.25°	1	Y	Y	Y	(Horowitz et al., 2020; Dunne et al., 2020; Krasting et al., 2018)

Formatted: Font: Not Bold

Formatted: Font: Not Bold

Formatted: Font: Not Bold

GISS-E2-1-OMA	2° × 2.5°	15	Y	Y	Y	(Bauer et al., 2020; Miller et al., 2021; Nasa Goddard Institute for Space Studies, 2018)
GISS-E2-1-MATRIX	2° × 2.5°	12	Y	Y		(Bauer et al., 2020; Miller et al., 2021; Nasa Goddard Institute for Space Studies, 2018)
HadGEM3-GC31-LL	1.25° × 1.875°	4	Y			(Ridley et al., 2018; Kuhlbrodt et al., 2018)
MIROC-ES2L	2.813° × 2.813°	10	Y		Y	(Hajima et al., 2020; Hajima et al., 2019)
MPI-ESM-1-2-HAM	1.875° × 1.875°	3	Y		Y	(Tegen et al., 2019; Neubauer et al., 2019)
MRI-ESM2-0	1.875° × 1.875°	5	Y		Y	(Yukimoto et al., 2019a; Yukimoto et al., 2019b; Oshima et al., 2020)
NorESM2-LM	1.9° × 2.5°	3	Y		Y	(Karset et al., 2018; Seland et al., 2019; Seland et al., 2020; Kirkevåg et al., 2018)
NorESM2-MM	0.9° × 1.25°	3	Y		Y	(Karset et al., 2018; Bentsen et al., 2019; Seland et al., 2020; Kirkevåg et al., 2018)
UKESM1-0-LL	1.25° × 1.875°	4	Y			(Tang et al., 2019; Sellar et al., 2019)

Table S2. The specific values of a_1 and a_2 from Eq. 1. The average, trend, and ~~trend~~spatial correlation coefficients of $PM_{2.5}$ concentrations over the eastern ~~regions~~region and western ~~regions~~region during 2000–2014.

	Model	a_1	a_2	Eastern ~~regions~~region Average ($\mu g\ m^{-3}$)	Eastern ~~regions~~region Trend ($\mu g\ m^{-3}\ yr^{-1}$)[a]	Eastern ~~regions~~region Spatial Corr.[b]	Western ~~regions~~region Average ($\mu g\ m^{-3}$)	Western ~~regions~~region Trend ($\mu g\ m^{-3}\ yr^{-1}$)	Western ~~regions~~region Spatial Corr.
Satellite-based				39.0	0.72	1	22.7	0.06*	1
Total $PM_{2.5}$ from Direct	GFDL-ESM4			37.7	1.14	0.92	22.1	0.28	0.66

Formatted: Font: Not Bold
Formatted: Font: Not Bold
Formatted: Font: Not Bold
Formatted: Font: Not Bold
Formatted: Font: Not Bold
Formatted: Font: Not Bold
Inserted Cells
Inserted Cells
Formatted: Indent: Hanging: 2.67 ch, Left -5.1 ch, First line: -2.67 ch
Merged Cells
Formatted: Line spacing: single
Formatted: Border: Right: (Single solid line, Background 1, 1.5 pt Line width)

ESM output								
	GISS-E2-1-OMA			24.4	0.69	0.91	10.9	0.13	0.79
	MIROC-ES2L			20.3	0.49	0.90	8.9	0.13	0.59
~~Total $PM_{2.5}$ from outputting~~	MPI-ESM-1-2-HAM			36.6	0.93	0.91	22.5	0.20*	0.36
	MRI-ESM2-0			30.4	0.57	0.83	24.5	0.24	0.71
	NorESM2-LM			22.1	0.32	0.87	35.5	0.03*	0.49
	NorESM2-MM			23.6	0.40	0.90	43.1	–0.10*	0.53
Total $PM_{2.5}$ from Eq. 1	BCC-ESM1			19.5	0.40	0.87	10.2	0.15	0.62
	CESM2-WACCM	0.25	0.1	24.0	0.73	0.92	10.1	0.22	0.67
	CNRM-ESM2-1	0.02	0.25	18.9	0.42	0.90	5.5	0.11	0.51
~~Total $PM_{2.5}$ from Eq. 1~~	EC-Earth3-AerChem	0.25	0.1	21.4	0.56	0.91	8.3	0.18	0.53
	GISS-E2-1-MATRIX	0.25	0.1	17.0	0.43	0.92	6.4	0.10	0.67
	HadGEM3-GC31-LL	0.27	0.35	26.5	0.80	0.89	7.9	0.18	0.50
	UKESM1-0-LL	0.27	0.35	26.5	0.71	0.89	8.1	0.18	0.52

[a] Trends are estimated using the Theil-Sen Median method (Theil, 1950; Sen, 1968). Significant changes are identified using the non-parametric Mann-Kendall test (Kendall, 1938). * represents non-significant monotonous change at p = 0.05. [b] Spatial correlation coefficients between simulations and satellite-based data over the eastern and western regions are calculated. The spatial correlation coefficients of 14 models are at the 0.05 significance level.

Table S3. Multi-year averages of $PM_{2.5}$ concentrations including five aerosol species (Eq. 1) and all fine aerosol species from 4 models providing nitrate and ammonium simulations.

Model	$PM_{2.5}$ according to	$PM_{2.5}$ including all	Nitrate	Ammonium

Formatted: Line spacing: single
Formatted: Line spacing: Multiple 1.15 li
Formatted: Line spacing: single
Formatted: Line spacing: single
Formatted: Line spacing: single
Formatted: Line spacing: single
Formatted: Line spacing: single
Formatted: Line spacing: single
Formatted: Line spacing: single
Formatted: Superscript

	Eq. 1 (μg m^{-3})	fine aerosol species (μg m^{-3})[a]	proportion[b]	proportion
EC-Earth3-AerChem	12.1	18.7	20.6%	14.3%
GFDL-ESM4	13.0	18.5	15.1%	14.6%
GISS-E2-1-OMA	10.0	14.1	17.6%	11.4%
GISS-E2-1-MATRIX	9.5	13.8	17.5%	13.2%

[a] represents that $PM_{2.5} = OA + BC + SO_4^{2-} + 0.25SSLT + 0.1DST + NO_3^- + NH_4^+$. [b] represents that the proportion of nitrate to $PM_{2.5}$ including all fine aerosol species.

Reference

Bauer, S. E., Tsigaridis, K., Faluvegi, G., Kelley, M., Lo, K. K., Miller, R. L., Nazarenko, L., Schmidt, G. A., and Wu, J.: Historical (1850–2014) Aerosol Evolution and Role on Climate Forcing Using the GISS ModelE2.1 Contribution to CMIP6, J. Adv. Model. Earth Syst., 12, e2019MS001978, https://doi.org/10.1029/2019MS001978, 2020.

Bentsen, M., Oliviè, D. J. L., Seland, Ø., Toniazzo, T., Gjermundsen, A., Graff, L. S., Debernard, J. B., Gupta, A. K., He, Y., Kirkevåg, A., Schwinger, J., Tjiputra, J., Aas, K. S., Bethke, I., Fan, Y., Griesfeller, J., Grini, A., Guo, C., Ilicak, M., Karset, I. H. H., Landgren, O. A., Liakka, J., Moseid, K. O., Nummelin, A., Spensberger, C., Tang, H., Zhang, Z., Heinze, C., Iversen, T., and Schulz, M.: NCC NorESM2-MM model output prepared for CMIP6 CMIP (v20201001), Earth System Grid Federation [dataset], https://doi.org/10.22033/ESGF/CMIP6.506, 2019.

Danabasoglu, G.: NCAR CESM2-WACCM model output prepared for CMIP6 CMIP (v20190415), Earth System Grid Federation [dataset], https://doi.org/10.22033/ESGF/CMIP6.10024, 2019.

Döscher, R., Acosta, M., Alessandri, A., Anthoni, P., Arsouze, T., Bergman, T., Bernardello, R., Boussetta, S., Caron, L. P., Carver, G., Castrillo, M., Catalano, F., Cvijanovic, I., Davini, P., Dekker, E., Doblas-Reyes, F. J., Docquier, D., Echevarria, P., Fladrich, U., Fuentes-Franco, R., Gröger, M., v. Hardenberg, J., Hieronymus, J., Karami, M. P., Keskinen, J. P., Koenigk, T., Makkonen, R., Massonnet, F., Ménégoz, M., Miller, P. A., Moreno-Chamarro, E., Nieradzik, L., van Noije, T., Nolan, P., O'Donnell, D., Ollinaho, P., van den Oord, G., Ortega, P., Prims, O. T., Ramos, A., Reerink, T., Rousset, C., Ruprich-Robert, Y., Le Sager, P., Schmith, T., Schrödner, R., Serva, F., Sicardi, V., Sloth Madsen, M., Smith, B., Tian, T., Tourigny, E., Uotila, P., Vancoppenolle, M., Wang, S., Wårlind, D., Willén, U., Wyser, K., Yang, S., Yepes-Arbós, X., and Zhang, Q.: The EC-Earth3 Earth system model for the Coupled Model Intercomparison Project 6, Geosci. Model Dev., 15, 2973-3020, https://doi.org/10.5194/gmd-15-2973-2022, 2022.

Dunne, J. P., Horowitz, L. W., Adcroft, A. J., Ginoux, P., Held, I. M., John, J. G., Krasting, J. P., Malyshev, S., Naik, V., Paulot, F., Shevliakova, E., Stock, C. A., Zadeh, N., Balaji, V., Blanton, C., Dunne, K. A., Dupuis, C., Durachta, J., Dussin, R., Gauthier, P. P. G., Griffies, S. M., Guo, H., Hallberg, R. W., Harrison, M., He, J., Hurlin, W., McHugh, C., Menzel, R., Milly, P. C. D., Nikonov, S., Paynter, D. J., Ploshay, J.,

Radhakrishnan, A., Rand, K., Reichl, B. G., Robinson, T., Schwarzkopf, D. M., Sentman, L. T., Underwood, S., Vahlenkamp, H., Winton, M., Wittenberg, A. T., Wyman, B., Zeng, Y., and Zhao, M.: The GFDL Earth System Model Version 4.1 (GFDL-ESM 4.1): Overall Coupled Model Description and Simulation Characteristics, J. Adv. Model. Earth Syst., 12, e2019MS002015, https://doi.org/10.1029/2019MS002015, 2020.

EC-Earth-Consortium: EC-Earth3-AerChem model output prepared for CMIP6 CMIP (v20201214), Earth System Grid Federation [dataset], https://doi.org/10.22033/ESGF/CMIP6.639, 2020.

Emmons, L. K., Schwantes, R. H., Orlando, J. J., Tyndall, G., Kinnison, D., Lamarque, J.-F., Marsh, D., Mills, M. J., Tilmes, S., Bardeen, C., Buchholz, R. R., Conley, A., Gettelman, A., Garcia, R., Simpson, I., Blake, D. R., Meinardi, S., and Pétron, G.: The Chemistry Mechanism in the Community Earth System Model Version 2 (CESM2), J. Adv. Model. Earth Syst., 12, e2019MS001882, https://doi.org/10.1029/2019MS001882, 2020.

Gettelman, A., Mills, M. J., Kinnison, D. E., Garcia, R. R., Smith, A. K., Marsh, D. R., Tilmes, S., Vitt, F., Bardeen, C. G., McInerny, J., Liu, H.-L., Solomon, S. C., Polvani, L. M., Emmons, L. K., Lamarque, J.-F., Richter, J. H., Glanville, A. S., Bacmeister, J. T., Phillips, A. S., Neale, R. B., Simpson, I. R., DuVivier, A. K., Hodzic, A., and Randel, W. J.: The Whole Atmosphere Community Climate Model Version 6 (WACCM6), J. Geophys. Res.-Atmos., 124, 12380-12403, https://doi.org/10.1029/2019JD030943, 2019.

Hajima, T., Watanabe, M., Yamamoto, A., Tatebe, H., Noguchi, M. A., Abe, M., Ohgaito, R., Ito, A., Yamazaki, D., Okajima, H., Ito, A., Takata, K., Ogochi, K., Watanabe, S., and Kawamiya, M.: Development of the MIROC-ES2L Earth system model and the evaluation of biogeochemical processes and feedbacks, Geosci. Model Dev., 13, 2197-2244, https://doi.org/10.5194/gmd-13-2197-2020, 2020.

Hajima, T., Abe, M., Arakawa, O., Suzuki, T., Komuro, Y., Ogura, T., Ogochi, K., Watanabe, M., Yamamoto, A., Tatebe, H., Noguchi, M. A., Ohgaito, R., Ito, A., Yamazaki, D., Ito, A., Takata, K., Watanabe, S., Kawamiya, M., and Tachiiri, K.: MIROC MIROC-ES2L model output prepared for CMIP6 CMIP (v20190823), Earth System Grid Federation [dataset], https://doi.org/10.22033/ESGF/CMIP6.902, 2019.

Horowitz, L. W., Naik, V., Paulot, F., Ginoux, P. A., Dunne, J. P., Mao, J., Schnell, J., Chen, X., He, J., John, J. G., Lin, M., Lin, P., Malyshev, S., Paynter, D., Shevliakova, E., and Zhao, M.: The GFDL Global Atmospheric Chemistry-Climate Model AM4.1: Model Description and Simulation Characteristics, J. Adv. Model. Earth Syst., 12, e2019MS002032, https://doi.org/10.1029/2019MS002032, 2020.

Karset, I. H. H., Berntsen, T. K., Storelvmo, T., Alterskjær, K., Grini, A., Olivié, D., Kirkevåg, A., Seland, Ø., Iversen, T., and Schulz, M.: Strong impacts on aerosol indirect effects from historical oxidant changes, Atmos. Chem. Phys., 18, 7669-7690, https://doi.org/10.5194/acp-18-7669-2018, 2018.

Kendall, M. G.: A new measure of rank correlation, Biometrika, 30, 81-93, https://doi.org/10.1093/biomet/30.1-2.81, 1938.

Kirkevåg, A., Grini, A., Olivié, D., Seland, Ø., Alterskjær, K., Hummel, M., Karset, I. H. H., Lewinschal,

907 A., Liu, X., Makkonen, R., Bethke, I., Griesfeller, J., Schulz, M., and Iversen, T.: A production-tagged
908 aerosol module for Earth system models, OsloAero5.3 – extensions and updates for CAM5.3-Oslo,
909 Geosci. Model Dev., 11, 3945-3982, https://doi.org/10.5194/gmd-11-3945-2018, 2018.

910 Krasting, J. P., John, J. G., Blanton, C., McHugh, C., Nikonov, S., Radhakrishnan, A., Rand, K., Zadeh,
911 N. T., Balaji, V., Durachta, J., Dupuis, C., Menzel, R., Robinson, T., Underwood, S., Vahlenkamp, H.,
912 Dunne, K. A., Gauthier, P. P. G., Ginoux, P., Griffies, S. M., Hallberg, R., Harrison, M., Hurlin, W.,
913 Malyshev, S., Naik, V., Paulot, F., Paynter, D. J., Ploshay, J., Reichl, B. G., Schwarzkopf, D. M., Seman,
914 C. J., Silvers, L., Wyman, B., Zeng, Y., Adcroft, A., Dunne, J. P., Dussin, R., Guo, H., He, J., Held, I. M.,
915 Horowitz, L. W., Lin, P., Milly, P. C. D., Shevliakova, E., Stock, C., Winton, M., Wittenberg, A. T., Xie,
916 Y., and Zhao, M.: NOAA-GFDL GFDL-ESM4 model output prepared for CMIP6 CMIP (v20190726),
917 Earth System Grid Federation [dataset], https://doi.org/10.22033/ESGF/CMIP6.1407, 2018.

918 Kuhlbrodt, T., Jones, C. G., Sellar, A., Storkey, D., Blockley, E., Stringer, M., Hill, R., Graham, T., Ridley,
919 J., Blaker, A., Calvert, D., Copsey, D., Ellis, R., Hewitt, H., Hyder, P., Ineson, S., Mulcahy, J., Siahaan,
920 A., and Walton, J.: The Low-Resolution Version of HadGEM3 GC3.1: Development and Evaluation for
921 Global Climate, J. Adv. Model. Earth Syst., 10, 2865-2888, https://doi.org/10.1029/2018MS001370,
922 2018.

923 Michou, M., Nabat, P., Saint-Martin, D., Bock, J., Decharme, B., Mallet, M., Roehrig, R., Séférian, R.,
924 Sénési, S., and Voldoire, A.: Present-Day and Historical Aerosol and Ozone Characteristics in CNRM
925 CMIP6 Simulations, J. Adv. Model. Earth Syst., 12, e2019MS001816,
926 https://doi.org/10.1029/2019MS001816, 2020.

927 Miller, R. L., Schmidt, G. A., Nazarenko, L. S., Bauer, S. E., Kelley, M., Ruedy, R., Russell, G. L.,
928 Ackerman, A. S., Aleinov, I., Bauer, M., Bleck, R., Canuto, V., Cesana, G., Cheng, Y., Clune, T. L., Cook,
929 B. I., Cruz, C. A., Del Genio, A. D., Elsaesser, G. S., Faluvegi, G., Kiang, N. Y., Kim, D., Lacis, A. A.,
930 Leboissetier, A., LeGrande, A. N., Lo, K. K., Marshall, J., Matthews, E. E., McDermid, S., Mezuman,
931 K., Murray, L. T., Oinas, V., Orbe, C., Pérez García-Pando, C., Perlwitz, J. P., Puma, M. J., Rind, D.,
932 Romanou, A., Shindell, D. T., Sun, S., Tausnev, N., Tsigaridis, K., Tselioudis, G., Weng, E., Wu, J., and
933 Yao, M.-S.: CMIP6 Historical Simulations (1850–2014) With GISS-E2.1, J. Adv. Model. Earth Syst., 13,
934 e2019MS002034, https://doi.org/10.1029/2019MS002034, 2021.

935 Nasa Goddard Institute for Space Studies: NASA-GISS GISS-E2.1G model output prepared for CMIP6
936 CMIP (v20190702), Earth System Grid Federation [dataset],
937 https://doi.org/10.22033/ESGF/CMIP6.1400, 2018.

938 Neubauer, D., Ferrachat, S., Siegenthaler-Le Drian, C., Stoll, J., Folini, D. S., Tegen, I., Wieners, K.-H.,
939 Mauritsen, T., Stemmler, I., Barthel, S., Bey, I., Daskalakis, N., Heinold, B., Kokkola, H., Partridge, D.,
940 Rast, S., Schmidt, H., Schutgens, N., Stanelle, T., Stier, P., Watson-Parris, D., and Lohmann, U.:
941 HAMMOZ-Consortium MPI-ESM1.2-HAM model output prepared for CMIP6 CMIP (v20190627),
942 Earth System Grid Federation [dataset], https://doi.org/10.22033/ESGF/CMIP6.1622, 2019.

943 Oshima, N., Yukimoto, S., Deushi, M., Koshiro, T., Kawai, H., Tanaka, T., and Yoshida, K.: Global and
944 Arctic effective radiative forcing of anthropogenic gases and aerosols in MRI-ESM2.0, Prog. Earth
945 Planet. Sci., 7, https://doi.org/10.1186/s40645-020-00348-w, 2020.

946 Ridley, J., Menary, M., Kuhlbrodt, T., Andrews, M., and Andrews, T.: MOHC HadGEM3-GC31-LL
947 model output prepared for CMIP6 CMIP (v20190624), Earth System Grid Federation [dataset],
948 https://doi.org/10.22033/ESGF/CMIP6.419, 2018.

949 Séférian, R.: CNRM-CERFACS CNRM-ESM2-1 model output prepared for CMIP6 CMIP (v20181206),
950 Earth System Grid Federation [dataset], https://doi.org/10.22033/ESGF/CMIP6.1391, 2018.

951 Séférian, R., Nabat, P., Michou, M., Saint-Martin, D., Voldoire, A., Colin, J., Decharme, B., Delire, C.,
952 Berthet, S., Chevallier, M., Sénési, S., Franchisteguy, L., Vial, J., Mallet, M., Joetzjer, E., Geoffroy, O.,
953 Guérémy, J.-F., Moine, M.-P., Msadek, R., Ribes, A., Rocher, M., Roehrig, R., Salas-y-Mélia, D.,
954 Sanchez, E., Terray, L., Valcke, S., Waldman, R., Aumont, O., Bopp, L., Deshayes, J., Éthé, C., and
955 Madec, G.: Evaluation of CNRM Earth System Model, CNRM-ESM2-1: Role of Earth System Processes
956 in Present-Day and Future Climate, J. Adv. Model. Earth Syst., 11, 4182-4227,
957 https://doi.org/10.1029/2019MS001791, 2019.

958 Seland, Ø., Bentsen, M., Olivié, D., Toniazzo, T., Gjermundsen, A., Graff, L. S., Debernard, J. B., Gupta,
959 A. K., He, Y. C., Kirkevåg, A., Schwinger, J., Tjiputra, J., Aas, K. S., Bethke, I., Fan, Y., Griesfeller, J.,
960 Grini, A., Guo, C., Ilicak, M., Karset, I. H. H., Landgren, O., Liakka, J., Moseid, K. O., Nummelin, A.,
961 Spensberger, C., Tang, H., Zhang, Z., Heinze, C., Iversen, T., and Schulz, M.: Overview of the Norwegian
962 Earth System Model (NorESM2) and key climate response of CMIP6 DECK, historical, and scenario
963 simulations, Geosci. Model Dev., 13, 6165-6200, https://doi.org/10.5194/gmd-13-6165-2020, 2020.

964 Seland, Ø., Bentsen, M., Oliviè, D. J. L., Toniazzo, T., Gjermundsen, A., Graff, L. S., Debernard, J. B.,
965 Gupta, A. K., He, Y., Kirkevåg, A., Schwinger, J., Tjiputra, J., Aas, K. S., Bethke, I., Fan, Y., Griesfeller,
966 J., Grini, A., Guo, C., Ilicak, M., Karset, I. H. H., Landgren, O. A., Liakka, J., Moseid, K. O., Nummelin,
967 A., Spensberger, C., Tang, H., Zhang, Z., Heinze, C., Iversen, T., and Schulz, M.: NCC NorESM2-LM
968 model output prepared for CMIP6 CMIP (v20190815), Earth System Grid Federation [dataset],
969 https://doi.org/10.22033/ESGF/CMIP6.502, 2019.

970 Sellar, A. A., Jones, C. G., Mulcahy, J. P., Tang, Y., Yool, A., Wiltshire, A., O'Connor, F. M., Stringer, M.,
971 Hill, R., Palmieri, J., Woodward, S., de Mora, L., Kuhlbrodt, T., Rumbold, S. T., Kelley, D. I., Ellis, R.,
972 Johnson, C. E., Walton, J., Abraham, N. L., Andrews, M. B., Andrews, T., Archibald, A. T., Berthou, S.,
973 Burke, E., Blockley, E., Carslaw, K., Dalvi, M., Edwards, J., Folberth, G. A., Gedney, N., Griffiths, P. T.,
974 Harper, A. B., Hendry, M. A., Hewitt, A. J., Johnson, B., Jones, A., Jones, C. D., Keeble, J., Liddicoat,
975 S., Morgenstern, O., Parker, R. J., Predoi, V., Robertson, E., Siahaan, A., Smith, R. S., Swaminathan, R.,
976 Woodhouse, M. T., Zeng, G., and Zerroukat, M.: UKESM1: Description and Evaluation of the U.K. Earth
977 System Model, J. Adv. Model. Earth Syst., 11, 4513-4558, https://doi.org/10.1029/2019MS001739, 2019.

978 Sen, P. K.: Estimates of the Regression Coefficient Based on Kendall's Tau, J. Am. Stat. Assoc., 63, 1379-
979 1389, https://doi.org/10.1080/01621459.1968.10480934, 1968.

980 Tang, Y., Rumbold, S., Ellis, R., Kelley, D., Mulcahy, J., Sellar, A., Walton, J., and Jones, C.: MOHC
981 UKESM1.0-LL model output prepared for CMIP6 CMIP (v20191011), Earth System Grid Federation
982 [dataset], https://doi.org/10.22033/ESGF/CMIP6.1569, 2019.

983 Tegen, I., Neubauer, D., Ferrachat, S., Siegenthaler-Le Drian, C., Bey, I., Schutgens, N., Stier, P., Watson-

Parris, D., Stanelle, T., Schmidt, H., Rast, S., Kokkola, H., Schultz, M., Schroeder, S., Daskalakis, N., Barthel, S., Heinold, B., and Lohmann, U.: The global aerosol–climate model ECHAM6.3–HAM2.3 – Part 1: Aerosol evaluation, Geosci. Model Dev., 12, 1643-1677, https://doi.org/10.5194/gmd-12-1643-2019, 2019.

Theil, H.: A Rank-Invariant Method of Linear and Polynomial Regression Analysis, Proc. R. Neth. Acad. Sci., 386–392,

Tilmes, S., Hodzic, A., Emmons, L. K., Mills, M. J., Gettelman, A., Kinnison, D. E., Park, M., Lamarque, J.-F., Vitt, F., Shrivastava, M., Campuzano-Jost, P., Jimenez, J. L., and Liu, X.: Climate Forcing and Trends of Organic Aerosols in the Community Earth System Model (CESM2), J. Adv. Model. Earth Syst., 11, 4323-4351, https://doi.org/10.1029/2019MS001827, 2019.

van Noije, T., Bergman, T., Le Sager, P., O'Donnell, D., Makkonen, R., Gonçalves-Ageitos, M., Döscher, R., Fladrich, U., von Hardenberg, J., Keskinen, J. P., Korhonen, H., Laakso, A., Myriokefalitakis, S., Ollinaho, P., Pérez García-Pando, C., Reerink, T., Schrödner, R., Wyser, K., and Yang, S.: EC-Earth3-AerChem: a global climate model with interactive aerosols and atmospheric chemistry participating in CMIP6, Geosci. Model Dev., 14, 5637-5668, https://doi.org/10.5194/gmd-14-5637-2021, 2021.

Wu, T., Zhang, F., Zhang, J., Jie, W., Zhang, Y., Wu, F., Li, L., Yan, J., Liu, X., Lu, X., Tan, H., Zhang, L., Wang, J., and Hu, A.: Beijing Climate Center Earth System Model version 1 (BCC-ESM1): model description and evaluation of aerosol simulations, Geosci. Model Dev., 13, 977-1005, https://doi.org/10.5194/gmd-13-977-2020, 2020.

Wu, T., Lu, Y., Fang, Y., Xin, X., Li, L., Li, W., Jie, W., Zhang, J., Liu, Y., Zhang, L., Zhang, F., Zhang, Y., Wu, F., Li, J., Chu, M., Wang, Z., Shi, X., Liu, X., Wei, M., Huang, A., Zhang, Y., and Liu, X.: The Beijing Climate Center Climate System Model (BCC-CSM): the main progress from CMIP5 to CMIP6, Geosci. Model Dev., 12, 1573-1600, https://doi.org/10.5194/gmd-12-1573-2019, 2019.

Yukimoto, S., Koshiro, T., Kawai, H., Oshima, N., Yoshida, K., Urakawa, S., Tsujino, H., Deushi, M., Tanaka, T., Hosaka, M., Yoshimura, H., Shindo, E., Mizuta, R., Ishii, M., Obata, A., and Adachi, Y.: MRI MRI-ESM2.0 model output prepared for CMIP6 CMIP historical (v20200218), Earth System Grid Federation [dataset], https://doi.org/10.22033/ESGF/CMIP6.6842, 2019a.

Yukimoto, S., Kawai, H., Koshiro, T., Oshima, N., Yoshida, K., Urakawa, S., Tsujino, H., Deushi, M., Tanaka, T., Hosaka, M., Yabu, S., Yoshimura, H., Shindo, E., Mizuta, R., Obata, A., Adachi, Y., and Ishii, M.: The Meteorological Research Institute Earth System Model Version 2.0, MRI-ESM2.0: Description and Basic Evaluation of the Physical Component, J. Meteorol. Soc. Jpn., 97, 931-965, https://doi.org/10.2151/jmsj.2019-051, 2019b.

Zhang, J., Wu, T., Shi, X., Zhang, F., Li, J., Chu, M., Liu, Q., Yan, J., Ma, Q., and Wei, M.: BCC BCC-ESM1 model output prepared for CMIP6 CMIP (v20191127), Earth System Grid Federation [dataset], https://doi.org/10.22033/ESGF/CMIP6.1734, 2018.

Formatted: Font: 10 pt, Not Bold

Formatted: EndNote Bibliography, Line spacing: single